# Tephra fallout probabilistic hazard maps for Cotopaxi and Guagua Pichincha volcanoes (Ecuador) with uncertainty quantification

A. Tadini[1], N. Azzaoui[2], O. Roche[1], P. Samaniego[1,3], B. Bernard[3], A. Bevilacqua[4], S. Hidalgo[3], A. Guillin[2], M. Gouhier[1]

[1]Université Clermont Auvergne, Laboratoire Magmas et Volcans, UCA-CNRS-IRD, 6 Avenue Blaise Pascal, 63178 Aubière, France.

[2]Université Clermont Auvergne, Laboratoire de Mathématiques Blaise Pascal, 3 place Vasarely, 63178 Aubière, France.

[3]Escuela Politécnica Nacional, Instituto Geofísico, Ladrón de Guevara E11-253 y Andalucía, Quito, Ecuador.

[4]Istituto Nazionale di Geofisica e Vulcanologia, Sezione di Pisa, via Cesare Battisti 53, 56125 Pisa, Italy.

Corresponding author: Alessandro Tadini (Alessandro.TADINI@uca.fr)

**Key Points:**

- We develop tephra fallout probabilistic hazard maps for Cotopaxi and Guagua Pichincha volcanoes using the PLUME-MoM/HYSPLIT model
- We incorporate the quantification of the uncertainty on the input parameters, the model, and the occurrence of different eruption types
- Our study indicates that full uncertainty quantification is essential in volcanic hazard assessment in order to provide robust information

**Index Terms and Keywords**

4314 Mathematical and computer modeling, 3275 Uncertainty quantification, 8428 Explosive volcanism, 8488 Volcanic hazards and risks

Tephra fallout, volcanic hazard assessment, Cotopaxi, Guagua Pichincha, uncertainty quantification

## Abstract

Tephra fallout hazard assessment is undertaken with probabilistic maps that rely on numerical models. Regarding maps production, the input parameters of the model (including atmospheric conditions), the physical approximations of the numerical simulations, and the probabilities of occurrence of different eruption types in specific time frames are among the most critical sources of uncertainty. We therefore present a tephra fallout hazard assessment study for two active volcanoes (Cotopaxi and Guagua Pichincha) in Ecuador. We utilize PLUME-MoM/HYSPLIT models, and a procedure for uncertainty quantification where: i) the uncertainty on eruptive source parameters and eruption type occurrence is quantified through expert elicitation; ii) we implement a new procedure for correlations between the different parameters, and iii) we use correction coeffients to take into account the uncertainty of the numerical model. Maps of exceedance probability given a deposit thickness threshold, and thickness maps given a probability of exceedence, are produced 1) for two eruptive scenarios (sub-plinian and Plinian) and 2) as a combination of these scenarios in case the next eruption will be sub-Plinian or Plinian. These maps are described according to the uncertainty distribution of eruption type occurrence probabilities, considering their $5^{th}$ percentile, mean, and $95^{th}$ percentile values. We finally present hazard curves describing exceeding probabilities in 10 sensitive sites within the city of Quito. Additional information includes the areal extent and the population potentially affected by different isolines of tephra accumulation. This work indicates that full uncertainty quantification helps in providing more robust scientific information, improving the hazard assessment reliability.



## Plain language summary

We present a tephra fallout (i.e., volcanic ash accumulation on the ground due to sedimentation from volcanic clouds) hazard assessment for two Ecuadorian volcanoes (Cotopaxi and Guagua Pichincha) threatening Quito, the capital city of Ecuador. The novelties of this study are that i) we use coupled models for eruptive column and ash transport and ii) we quantify the main sources of uncertainties that normally affect probabilistic hazard maps. In particular, we present probability maps , for which a certain deposit thickness is overcome, and thickness maps, which show the expected thickness for a given probability. For the two volcanoes, the maps are related to the case that a next eruption will be of medium to large size (i.e. sub-Plinian or Plinian). Moreover, we also present hazard curves for 10 sensitive sites within the city of Quito. These curves are used to infer, for each site, the probabilities for a given accumulation of ash. Finally, we show the areal extent and the poupulation potentially affected by different tephra accumulations. Our study points toward the necessity to perform a full uncertainty quantification for volcanic hazard assessment.


## 1 Introduction

Among the numerous hazards related to volcanic eruptions, tephra fallout is certainly one of the most severe because it may affect large areas (> 100 $km^2$; Blong, 1996) and has a dramatic impact on both human settlements and activities (Brown *et al.*, 2017). While tephra residence in the atmosphere can lead to near-total disruption of air traffic over a vast region (e.g., Eyjafjallajokull 2010 eruption; Budd *et al.*, 2011; Bursik *et al.*, 2009; Folch *et al.*, 2012; Folch & Sulpizio, 2010), tephra accumulation on the ground affects human health (Baxter, 1990; Baxter & Horwell, 2015), buildings stability (Macedonio & Costa, 2012; Spence *et al.*, 2005),

roads/transportation systems (Blake *et al.*, 2017; Guffanti *et al.*, 2009), electrical infrastructure (Bebbington *et al.*, 2008; Wilson *et al.*, 2014), farmland/livestock (Annen & Wagner, 2003) or water reservoirs and vegetation (Wilson *et al.*, 2012). In response to such threats, numerous researches have been carried out for providing authorities, stakeholders and population with tools for both volcanic crises management and long-term urban planning. Particularly, in this latter case, tephra fallout hazard maps have been produced using different strategies that rely on field data of past eruptions (e.g., Orsi *et al.*, 2004) or which combine field data and numerical modelling (Barberi *et al.*, 1990; Bursik, 2001; Cioni *et al.*, 2003; Macedonio *et al.*, 1988).This latter approach is normally coupled with semi-probabilistic to fully probabilistic Monte Carlo techniques (Hurst & Smith, 2004) to sample model input parameters, and takes advantage of the great availability of tephra transport and deposition numerical models. As examples, tephra fallout hazard maps have been produced using different models such as HAZMAP (Bonasia *et al.*, 2011; Capra *et al.*, 2008; Costa *et al.*, 2009; Macedonio *et al.*, 2005), TEPHRA2 (Biass & Bonadonna, 2013; Biass *et al.*, 2014; Bonadonna *et al.*, 2005; Tsuji *et al.*, 2017; Yang *et al.*, 2021), FALL3D (Costa *et al.*, 2006; Folch *et al.*, 2009; Folch *et al.*, 2020; Prata *et al.*, 2021; Scaini *et al.*, 2012; Vázquez *et al.*, 2019), VOL-CALPUFF (Barsotti *et al.*, 2018; Barsotti & Neri, 2008; Barsotti *et al.*, 2008) and ASH3D (Alpízar Segura *et al.*, 2019; IG-EPN *et al.*, 2019; Schwaiger *et al.*, 2012; Yang *et al.*, 2020) models. The key elements for the modelling of tephra dispersal and for the development of probabilistic maps are: i) the identification of the eruptive scenarios that describe the eruptive history of the volcano; ii) the quantification of the uncertainty range of the eruptive source parameters (ESPs) related to each scenario; and iii) the estimation of the temporal recurrence rate and/or the probability of occurrence of the identified scenarios within defined temporal frames (Sandri *et al.*, 2016). Especially for the last two elements, uncertainty was quantified in recent hazard-related studies mostly through comparison between available field data and existing global volcanological databases (see for example Biass & Bonadonna, 2013). How the input uncertainty propagates through the model, and how it is influenced by wind field variability has been the topic of several studies (Bursik *et al.*, 2012; Macedonio *et al.*, 2016; Madankan *et al.*, 2014; Pouget *et al.*, 2016; Scollo *et al.*, 2008; Stefanescu *et al.*, 2014). An important source of uncertainty that has a direct impact on final map production has been however poorly considered so far, that is, the uncertainty related to the inadequacy of the numerical model itself, which is linked to the necessary physical approximations (including neglected physical processes) that allow acceptable computational times. Constraining the model-related uncertainty is an open challenge in common with other geophysical mass flow modeling efforts, and requires a statistically-based and multi-model approach (Bevilacqua *et al.*, 2019; Costa *et al.*, 2016b; Patra *et al.*, 2020; Patra *et al.*, 2018).

This paper presents a tephra fallout hazard assessment study, which focuses on the area of Quito, Ecuador's capital city. In order to perform this study, we focus on Cotopaxi and Guagua Pichincha, which are located nearby the city and are currently active volcanoes with recent eruptions. To develop probabilistic hazard maps, we employ a model that is the result ofa coupling between the plume model PLUME-MoM (de'Michieli Vitturi *et al.*, 2015) and the tephra dispersal model HYSPLIT (Stein *et al.*, 2015), as already performed by Tadini *et al.* (2020) and Pardini *et al.* (2020). There have not been so far any attempts to use this coupled model to produce probabilistic hazard maps for tephra fallout, although HYSPLIT is currently used by several Volcanic Ash Advisory Centers (Mastin *et al.*, 2017) for operational_purposes: this study is therefore a first step to a broader usage of this model outside the domain of real-time tracking of volcanic particles. The main novelty of this study is the implementation of a

procedure that takes into account three major sources of uncertainty during the production of tephra fallout hazard maps (on the ESPs, the model, and the eruption type occurrence probability). Particularly, the definition of these uncertainties has been the topic of two precedent studies (Tadini *et al.*, 2020, 2021)developed in the framework of the same research project (see Acknowledgements).

We firstly introduce Cotopaxi and Guagua Pichincha volcanoes (section 2). Then we describe the modelling strategy (section 3.1), the uncertainty quantification for ESPs and eruption type occurrence (section 3.2), and the procedure for hazard maps and hazard curves production. Finally, section 4 focuses on the presentation of the maps/curves and on the discussion of their main implications, including the areas and the people potentially involved by each hazard isoline.

## 2 Background

Quito, Ecuador's capital city, is located in the inter-andean valley, within the province of Pichincha (Fig. 1a). With almost three millions of inhabitants it is also the largest city in the country, it hosts the largest airport in Ecuador and it is in the middle of the most important road systems (e.g. the "Pan-American highway"; Fig. 1a).

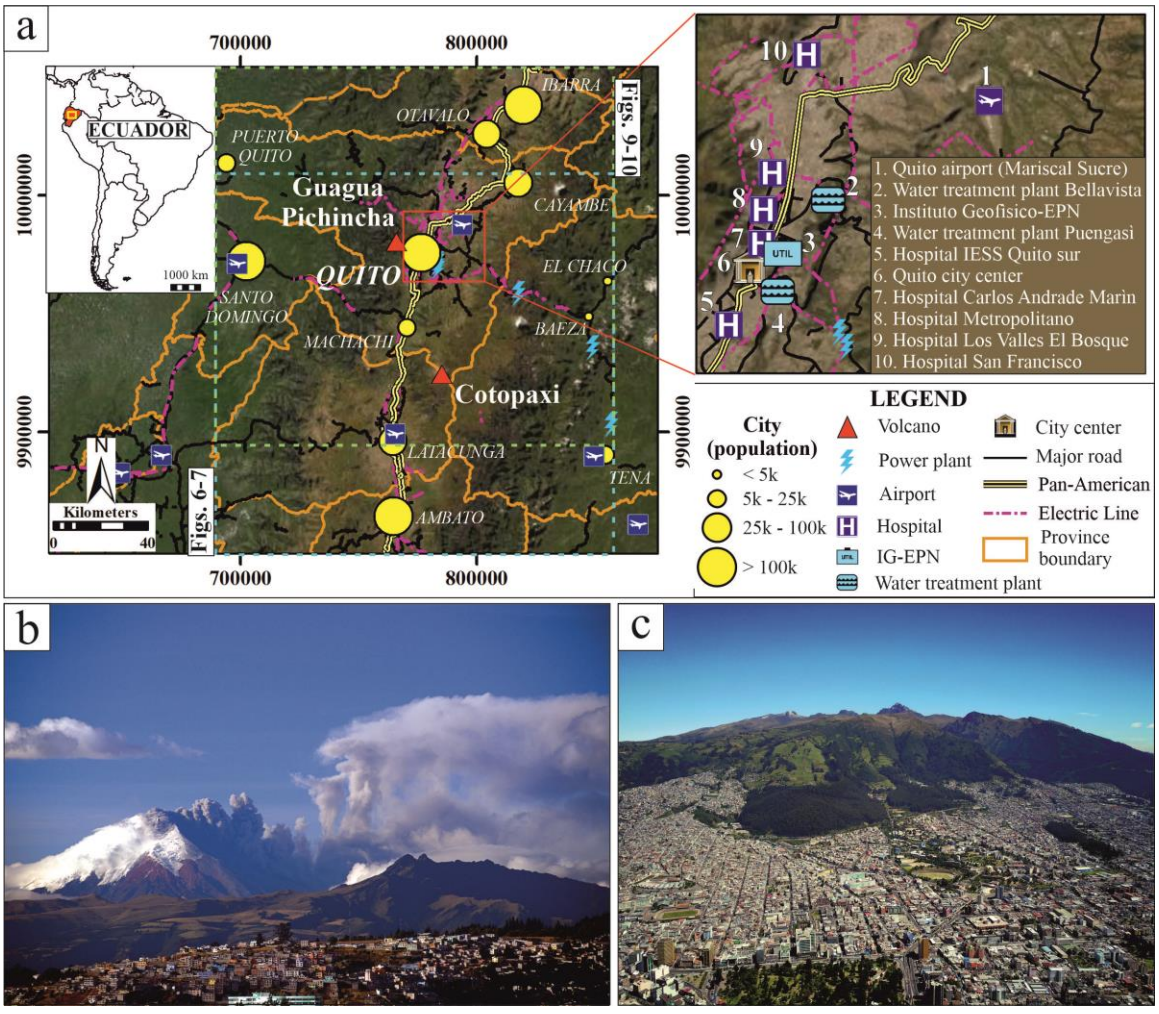

**Figure 1.** a) Location of Cotopaxi and Guagua Pichincha volcanoes with respect to the capital city Quito and the main towns and infrastructures in the region. Light blue and light green dashed boxes represent, respectively, the extents of Figs. 6-7 and 9-10; sensitive sites within the capital city of Quito considered in this study are shown. Coordinates are in the UTM WGS84 17S system. Service Layer Credits, source: Esri, DigitalGlobe, GeoEye, Earthstar Geographics, CNES/Airbus DS, USDA, USGS, AeroGRID, IGN and the GIS User Community; b) Cotopaxi volcano seen from North; c) Guagua Pichincha volcanic complex and the city of Quito seen from East.

### 2.1 Cotopaxi

According to Hall & Mothes (2008), the eruptive history of Cotopaxi volcano (Fig. 1a and b) began about 500 ka and has been firstly characterized by dome-forming to Plinian eruptions (up to VEI 4-5 or greater), which erupted mostly rhyolitic magmas (70–75 wt.% $SiO_2$). In contrast, from ~4 ka until present day, magmas erupted were almost all andesitic in composition (56–62 wt.% $SiO_2$). The latter period of activity (i.e. the last 2000 years) with andesitic magmas include violent Strombolian VEI 2-3 (in the XIX century, Pistolesi *et al.*, 2011), sub-Plinian VEI 3-4 (AD 1877 or XVIII century, Pistolesi *et al.*, 2011) and Plinian VEI 4-5 (Layer 3/X, 820±80 years BP; Layer 9/5/L-2, 1,180±80 years BP; Barberi *et al.*, 1995; Biass & Bonadonna, 2011; Hall & Mothes, 2008) eruptions. The last eruption of Cotopaxi is the AD 2015 VEI 1-2 eruption, characterized by an opening hydrovolcanic phase followed by a ~3 months long ash emission, which erupted a total of ~ $8.6 \times 10^5$ $m^3$ of tephra and caused a severe air traffic disturbances and impacted rural activities in the region (Bernard *et al.*, 2016; Gaunt *et al.*, 2016; Hidalgo *et al.*, 2018).

Cotopaxi volcano has been the subject of tephra fallout hazard assessment studies (Biass & Bonadonna, 2013; Hall *et al.*, 2004a; Hall *et al.*, 2004b; Hall & von Hillebrandt, 1988a; Miller *et al.*, 1978) and risk (Biass *et al.*, 2013). Particularly, Biass & Bonadonna (2013) performed a probabilistic tephra fallout hazard assessment for five eruption types (two with fixed ESPs and three with ESPs defined as a variation range), with magnitudes ranging from VEI 3 to 5. For each eruption type, 1,000 runs were carried out by using the TEPHRA2 model. As input parameters for this model, Biass & Bonadonna (2013) considered, for each run, i) a wind profile sampled from the NOAA NCEP/NCAR Reanalysis 1 database (Kalnay *et al.*, 1996) and ii) erupted volume, plume height and median grainsize sampled from a specific distribution. The probability of tephra accumulation in a given time window was presented by the authors through three different outputs, i) probability maps for a given tephra accumulation, ii) isomass maps for a given probability value and iii) hazard curves of tephra load for several locations, including Quito city center and the town of Latacunga. The authors calculated also the probability of occurrence of an eruption of VEI $\geq 3$ for the next 10 (~36%) and 100 (~99%) years. Biass *et al.* (2013) performed instead a risk assessment for eruptions with VEI $\geq 4$, and highlighted the possibility of roof collapse due to tephra loading of several thousands of houses in the proximity of the volcano, the destruction of agriculture and the possible disruption of major roads. Later, Volentik & Houghton (2015) performed a more extended hazard assessment focused on the potential impact of tephra fallout on Quito International airport from explosive eruptions of different Ecuadorian volcanoes. They used the TEPHRA2 model and NCEP/NCAR Reanalysis 1 wind data, while plume height, eruption duration, total mass and median/sorting of grain size were sampled from uniform, log-uniform or log-normal distributions. Specifically for Cotopaxi, the study indicated, at Quito airport, a yearly probability of mass accumulation of 1 mm and 10 mm of, respectively, ~14% and 2.5%. Recently, a multi-hazard map for Cotopaxi was released

184 divided in three sectors, North (Mothes *et al.*, 2016a), South (Mothes *et al.*, 2016b) and East
185 (Vasconez *et al.*, 2017). In the first two maps, tephra fallout hazard assessment was treated as the
186 expected tephra accumulation (with thresholds of 5 and 25 cm) in case of an eruption with VEI
187 3-5, based on field data of past eruptions with similar magnitudes. In the map of Vasconez *et al.*
188 (2017), instead, the authors presented the most likely (80%) distribution for a VEI 3 eruption
189 (similar to the AD 1877) based on 120 simulations (1 per month for 10 years, windfield
190 reanalysis 2007-2017) using the ASH3D model (Schwaiger *et al.*, 2012). In this map, Quito is
191 potentially (<20% probability) affected by ashfall deposits of thickness between 10 and 100 mm.
192 Finally, additional tephra fallout maps have been presented in the work of Cruz Roja Ecuatoriana
193 (2020), which includes maps for 5 eruptive scenarios (120 simulations each using the ASH3D
194 model) for different probability thresholds (1, 25, 50, 75 and 99%)

195 2.2 Guagua Pichincha

196 The Pichincha volcanic complex (Fig. 1a and c) is composed of three distinct edifices, the
197 youngest of which is Guagua Pichincha (4,784 m a.s.l.). During the eruptive history of this latter
198 (starting from 60 ka), all the erupted products were of andesitic to dacitic composition (59-66
199 wt.% $SiO_2$; Robin *et al.*, 2010). Guagua Pichincha volcano has been affected by two major sector
200 collapses (at ~11 ka and ~4 ka): after the latter one ("Toaza" sector collapse; Robin *et al.*, 2008)
201 the eruptive history has been characterized mainly by phases of growth and destruction of a
202 dome complex located in the landslide scar ("Cristal Dome"). From ~4 ka up to AD 1660, Robin
203 *et al.* (2008) recognized three major eruptive cycles that occurred during the 1$^{st}$ and 10$^{th}$ century,
204 and in AD 1660 (named respectively "I century", "X century" and "Historic"), each of them
205 separated from the others by repose times of the order of hundreds of years. Each cycle was
206 initiated with effusive, dome-forming eruptions alternated with low-magnitude vulcanian
207 episodes, and was closed by a final, medium-large magnitude (VEI 3-4) sub-Plinian to Plinian
208 eruption (Robin *et al.*, 2008). The eruption that ended the Historic cycle occurred in AD 1660
209 (Robin *et al.*, 2008) and caused severe tephra fallout in Quito and pyroclastic density currents on
210 the western side of the volcano (Wolf, 1904). After more than 300 years of quiescence, volcanic
211 activity at Guagua Pichincha started over in AD 1999, lasting for almost two years until AD
212 2001. This period, which included several Vulcanian events and a series of dome-forming
213 eruptions (Garcia-Aristizabal *et al.*, 2007; Wright *et al.*, 2007), might represent the beginning of
214 a new eruptive cycle like those cited in Robin *et al.* (2008).

215 The first tephra fallout hazard assessments at Guagua Pichincha have been done by Hall
216 & von Hillebrandt (1988b) and Barberi *et al.* (1992). Particularly, the latter authors considered
217 the Plinian eruptions of the X century and Historic cycles as the events with the maximum size
218 among those potentially expected in the future, and they calculated the expected tephra
219 accumulation using the model of Armienti *et al.* (1988). For this model they considered two
220 single meteorological profiles (i.e. wind) and specific eruptive source parameters for each of the
221 two eruptions. Resulting maps described tephra accumulation in term of thickness (from 5 to 50
222 cm) and a zonation of the area surrounding Guagua Pichincha in different classes according to
223 the impact of tephra fall and other volcanic-related hazards. Volentik & Houghton (2015), in the
224 case of an eruption from Guagua Pichincha volcano, indicated at Quito airport a probability of
225 accumulation of 1 mm and 10 mm of ash of 17.5 and 7 %, respectively. Finally, a multi-hazard
226 map for Guagua Pichincha was published (IG-EPN *et al.*, 2019) within the already cited work of
227 Cruz Roja Ecuatoriana (2020). For this map, the ASH3D model has been used (Schwaiger *et al.*,
228 2012), and tephra fallout hazard assessment has been treated in a semi-probabilistic way. Three
229 scenarios linked to three past eruptions (AD 1999-2001, AD 1660-Historic, X century) have

been considered with fixed eruptive source parameters, while wind profiles were statistically sampled at each iteration. Resulting maps described the expected tephra thickness (in mm) for given probabilities (1, 25, 50, 75 and 99%).

# 3 Methods

## 3.1 Numerical modelling

### 3.1.1 PLUME-MoM/HYSPLIT model

After its first release (de'Michieli Vitturi *et al.*, 2015), PLUME-MoM has been recently upgraded to a new version (PLUME-MoM-TSM, with "TSM" standing for "two-sized moments"; de' Michieli Vitturi & Pardini, 2021). This model describes the steady-state dynamics of a plume in 3D coordinates through a system of equations for the conservation of mass, momentum, energy, and the variation of heat capacity and mixture gas constant. The model considers radial and crosswind air entrainment, and it adopts the method of moments to describe a continuous size distribution of one or more group of particles (e.g., with different densities, shapefactors,etc.). Moreover, PLUME-MoM-TSM can simulate, for sustained eruptions, the initial spreading of the umbrella cloud due to the development of gravity currents originating from the plume overshoot (i.e. above the neutral buoyancy level). This feature allows a more detailed computation of the spreading of the umbrella cloud, especially in its upwind part. In PLUME-MoM-TSM, the amount of mass released is computed i) along the plume centerline, at emission points located at fixed height; ii) from the area defined by the umbrella cloud. Both the emission points and the umbrella cloud area represent the source locations for HYSPLIT.

HYSPLIT (Stein *et al.*, 2015) is an atmospheric dispersion model that describes the advection/diffusion of air parcels considering a Lagrangian approach and that computes the concentrantion/sedimentation of pollutants (volcanic particles in our case) at fixed receptors (Eulerian approach). The dispersion of a pollutant is described by assuming three types of configuration, “3D particles”, “puff” or hybrid configurations between the two. Particularly, while a 3D particle is a point mass transported by the wind that does not grow or split, a “puff” represents the distribution of a large number of 3D particles with a predefined concentration distribution in both the horizontal and vertical directions. The puffs expand with atmospheric turbulence, and if they exceed the size of the meteorological grid cell they are split into several new puffs, each with their respective pollutant mass. We have used the hybrid configuration, which considers 2D objects with zero vertical depth and planar mass. In this way, such objects move horizontally according to the “puff” configuration, while in the vertical direction they move like 3D particles (i.e. they do not expand nor split) mostly depending on the terminal fall velocity of the pollutant. As discussed in Tadini *et al.* (2020) this configuration allows use of a limited number of puffs (thus reducing computationl times) to properly capture both the horizontal dispersion and the vertical wind shears. In this work we have used the April 2018 release version of HYSPLIT, with the modifications detailed in Tadini *et al.* (2020).

### 3.1.2 Uncertainty quantification for the numerical model

In this paper we apply the procedure for the quantification of the uncertainty of tephra fallout model described in Tadini *et al.* (2020). In the latter, the coupled PLUME-MoM/HYSPLIT model has been used to reproduce four past eruptions from Tungurahua and

Cotopaxi volcanoes (in Ecuador) and Puyehue-Cordón Caulle volcano (in Chile). Input parameters for these eruptions have been collected after a thorough literature review, as well as from ground deposit and plume height measurements. The uncertainty was quantified by computing the differences between modeled and observed data of plume height above the vent, and mass loading and grain size at given stratigraphic sections. Regarding mass loading ($kg/m^2$) in particular, for each eruption type and meteorological dataset tested, Tadini *et al.* (2020) calculated the model mean overestimation (MO) and the mean underestimation (MU),

$$\begin{cases} MO = \frac{\sum_{i=1}^{N_o} \Delta_i}{N_o} \ \ for\ \Delta_i > 0 \\ MU = \frac{\sum_{i=1}^{N_u} \Delta_i}{N_u} \ \ for\ \Delta_i < 0 \end{cases} \quad (1)$$

where Δ is the difference between the computed and the observed values of mass loading (in $kg/m^2$) evaluated for sections with indexes from i=1 to, respectively, $N_o$ and $N_u$. These latter are the numbers of sections with overestimation and underestimation, respectively. MO and MU values were divided by the mean value of mass loading measured in the field for all the considered sections (MML), thus giving two coefficients (MO/MML and MU/MML), which we will use in section 3.3.1 to account for, respectively, model overestimation and underestimation. This approach has the advantage of summarizing the errors in two coefficients. However, we note the average of differences at all the sections may be far from representative of the errors at the sites with greatest or lowest accumulations. Results of the study of Tadini *et al.* (2020) highlight that: i) the model tends to have (for larger magnitude eruptions) a higher degree of overestimation rather than understimation (i.e. MO/MML > MU/MML); ii) sections with underestimation tend to be both in more proximal and medial/distal locations from the vent, while sections with overestimation tend to be more concentrated in proximal/medial locations mostly along the main dispersal axis of the deposit; iii) among the different tested meteorological datasets, none of them is systematically better than the others in minimzing the differences between modeled and observed mass loading values. With respect to this latter point, the authors showed also that the employment of more spatially and temporally refined meteorological datasets do not always improve the result.

Given the new features introduced in PLUME-MoM (see Section 3.1.1), we ran the simulations again for the two eruptions with the largest size (in terms of magnitude) used by Tadini *et al.* (2020), which are Tungurahua 2006 (sub-Plinian, VEI 3-4; Eychenne *et al.*, 2012) and Puyehue-Cordón Caulle 2011 (sub-Plinian, VEI 4; Bonadonna *et al.*, 2015a). For these eruptions we have used the same input parameters as those used by Tadini *et al.* (2020) along with the GDAS meteorological dataset (to be consistent with the one used in this work, see section 3.2.2). In order to take into account the full uncertainty of the model, we chose the two MO/MML and MU/MML largest values, , which were

MO/MML = 1.48
MU/MML = -0.49

These two values are related to the Puyehue-Cordón Caulle 2011 sub-Plinian eruption simulated using the GDAS meteorological data. As a comparison, the two values from Tadini *et al.* (2020) are larger (MO/MML = 3.15; MU/MML = -1.03), highlighting how the features introduced with the new version of PLUME-MoM have allowed reduction of the uncertainty of the model.

## 3.2 Eruption type probabilities and input parameters for the numerical model

### 3.2.1 Eruption type probabilities

To provide a quantification of the uncertainty in future eruption occurrences at both Cotopaxi and Guagua Pichincha volcanoes, Tadini *et al.* (2021) performed an expert elicitation session aimed at quantifying such values, which we will use in the merging of maps/curves (see section 3.3.3). In general, during an elicitation session (Aspinall, 2006; Aspinall *et al.*, 2019; Bevilacqua *et al.*, 2015; Neri *et al.*, 2008; Tadini *et al.*, 2017a) selected experts are asked to provide their judgements (in the form of three percentiles, normally the $5^{th}$, $50^{th}$ and $95^{th}$) on two different questionnaires. Firstly, they are asked factual questions with known answers to the organizers, to which they answer by providing credible intervals that capture the 'true' values (seed questions). The score that each expert got assigned after filling this first questionnaire is then used to pool all experts' judgements on a second questionnaire. This questionnaire enlists a number of "target" questions with unknown answers, which specifically address the problem(s) under investigation, in order to obtain group synthesized answers called 'decision-maker'.

In Tadini *et al.* (2021), a total of 20 experts (with different background, experience and knowledge on the studied volcanoes) were calibrated through 14 seed questions on south American (particularly Ecuadorian) volcanism and numerical modelling of tephra transport and dispersal. Thus the experts were weighted using two performance-based schemes: the CM (Classical Model, Cooke, 1991) and ERF (Expected Relative Frequency, Flandoli *et al.*, 2011) methods, and compared to an equal weight combination. The experts were then asked to provide their answers on 55 target questions on both future eruption occurrences and eruptive source parameter uncertainty ranges (see section 3.2.2). Regarding future eruption occurrences, two time frames were distinguished: the next eruption and the next 100 years. The former was aimed at assessing what would be the probability for the next eruption of a specific type (the mean elicited values summed up to 100%), while the 100 years focused on the probability of having at least one eruption of a specific type within the next 100 years (no constraints on the elicited values sum). This was made in order to consider the case of new large scale eruptions in the next 100 years, albeit preceded by smaller size events. The comparison to previous estimates based on temporal models of the eruptive record is thoroughly discussed in Tadini et al. (2021). A major advance was related to having obtained a probability distribution of eruption occurrence over an uncertainty range, thus enabling a doubly stochastic approach (Bevilacqua *et al.*, 2020; Bevilacqua *et al.*, 2018; Bevilacqua *et al.*, 2016; Marzocchi *et al.*, 2008; 2010; Neri *et al.*, 2008; Tadini *et al.*, 2017b). The concept of "probability of probability" is the key to assess the epistemic uncertainty affecting the probability of occurrence of eruption types, thus having implications on the entire subsequent hazard assessment. This concept is opposed to the aleatoric uncertainty expressed by these probabilities. More details on this topic may be found in the above-mentioned studies.

In this paper we use the results related to the CM model, and the corresponding probability distributions for the eruption types considered in this study (i.e. sub-Plinian and Plinian) are reported in Fig. 2.

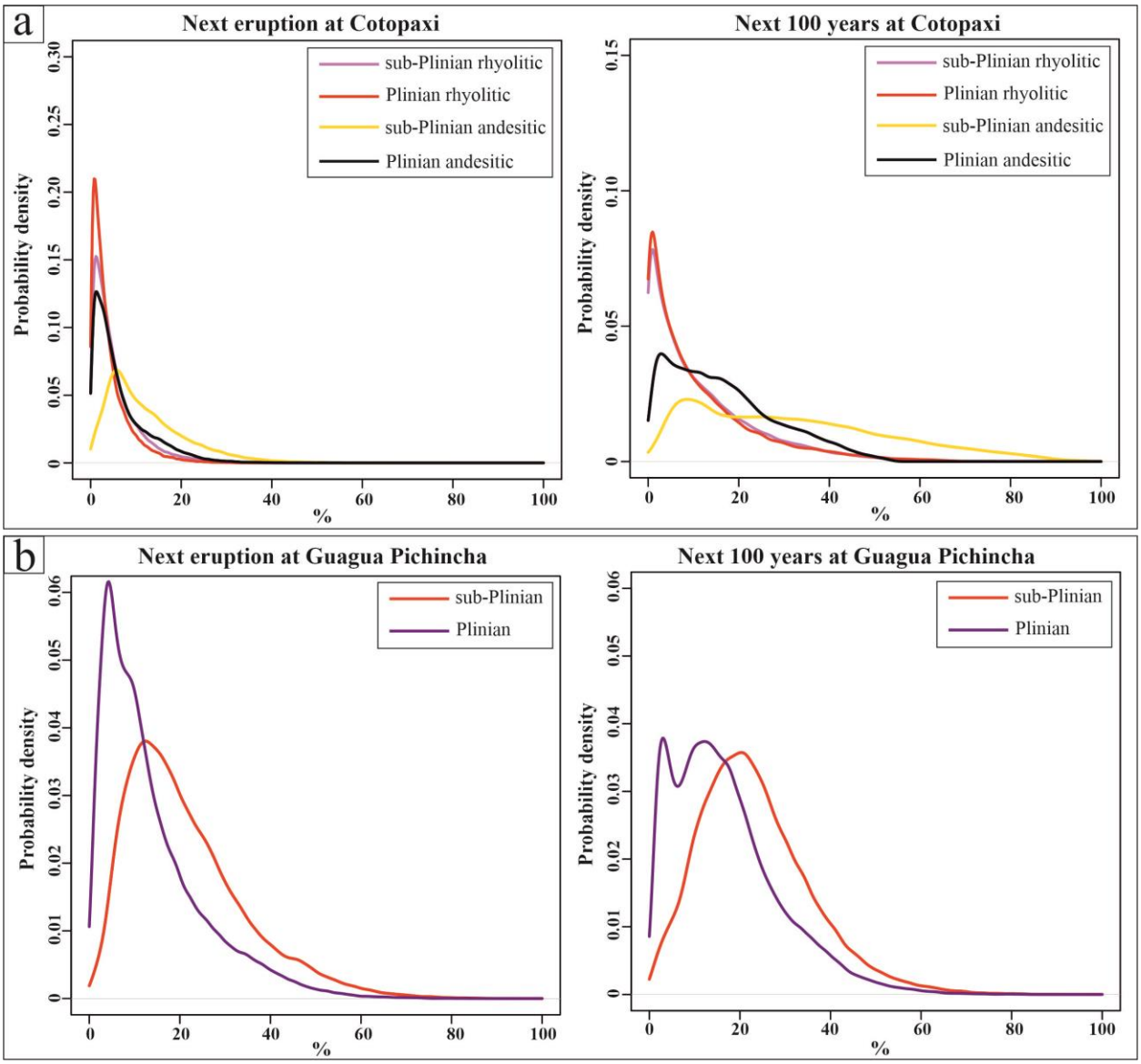


**Figure 2**. Uncertainty distributions according to the Classical Model method for the probability of occurrences of the sub-Plinian and Plinian eruption types for a) Cotopaxi and b) Guagua Pichincha volcanoes. For both volcanoes the uncertainty distributions are shown fori) the probability that next eruption will be either sub-Plinian or Plinian (left panels) and ii) the probability that there will be at least one eruption of each size within the next 100 years (right panels). y-axis describes the density of the probability density function. Data from Tadini *et al.* (2021).

Mean values of the probability distributions are reported in Table 1, while the three percentiles for each eruption type are reported in Table S1 from the supporting information. For Cotopaxi, the graphs of Fig. 2 and the mean probabilities of Table 1 indicate that eruptions involving rhyolic magmas are less probable than their andesitic counterparts for the next eruption but also in the next 100 years time frames. However, the mean probability that the next eruption will involve a rhyolitic magma is not negligible (10.5% - Table 1). We note that sub-Plinian and Plinian eruptions give a summed mean probability of occurrence for the four eruption types of

~29%, while for Guagua Pichincha the sum of the mean probabilities for sub-Plinian and Plinian is 36% (see Table 1).

| **Eruption Cotopaxi** | **Next eruption (%)** | **Next 100 years (%)** |
|---|---|---|
| *sub-Plinian Rhyolitic* | 5.9 | 12 |
| *Plinian Rhyolitic* | 4.6 | 12 |
| *sub-Plinian Andesitic* | 12 | 31 |
| *Plinian Andesitic* | 6.9 | 17 |
| **Eruption Guagua Pichincha** | **Next eruption (%)** | **Next 100 years (%)** |
| *sub-Plinian* | 22 | 28 |
| *Plinian* | 14 | 21 |

**Table 1**. Mean values of the distributions of Figure 2. Data from Tadini *et al.* (2021).

3.2.2 Input parameters for the numerical model

We used uncertainty distributions to sample three important parameters for tephra fallout hazard assessment and numerical modeling, which are eruption duration, total mass of the fallout deposit, and average plume height. Such distributions were defined by the expert elicitation session thoroughly described in Tadini *et al.* (2021) and summarized in section 3.2.1. We report these uncertainty distributions in Fig. 3 and the mean values of such distributions in Table 2, while the three elicited percentiles ($5^{th}$, $50^{th}$, and $95^{th}$) are reported in Tables S1 and S2 from the supporting information.

| **Eruption Cotopaxi** | **Duration [hours]** | **Total mass fallout [$10^9$ kg]** | **Average plume height [km]** | **MdΦ** | **σΦ** |
|---|---|---|---|---|---|
| *sub-Plinian Rhyolitic* | 3.3 (4.1) | 49 (36) | 14 (18) | -0.5 - 4 | 2.1 - 3.1 |
| *Plinian Rhyolitic* | 6.2 (7.6) | 270 (365) | 22 (27) | -0.4 - 4 | 2 - 3.3 |
| *sub-Plinian Andesitic* | 1.8 (3.8) | 27 (31) | 16 (17) | -1.2 - 4.5 | 1.7 - 3.4 |
| *Plinian Andesitic* | 2.2 (7.7) | 240 (262) | 24 (24) | -0.8 - 4.4 | 1.8 - 3.3 |
| **Eruption Guagua Pichincha** | **Duration [hours]** | **Total mass fallout [$10^9$ kg]** | **Average plume height [km]** | **MdΦ** | **σΦ** |
| *sub-Plinian* | 2.2 (3.8) | 24 (25) | 16 (16) | 1.3 - 3.8 | 2.2 -3.3 |
| *Plinian* | 4 (7) | 130 (150) | 24 (21) | 1.5 - 3.7 | 2.1 - 3.2 |

**Table 2**. Mean values for duration, total fallout mass and average plume height (Figure 3 and Tadini *et al.*, 2021) and maximum-minimum values for median (MdΦ) and sorting (σΦ) of the total grain-size distributions (Costa *et al.*, 2016a). Values in parenthesis are mean values after the application of the relation of Mastin *et al.* (2009) described in section 3.3.1.

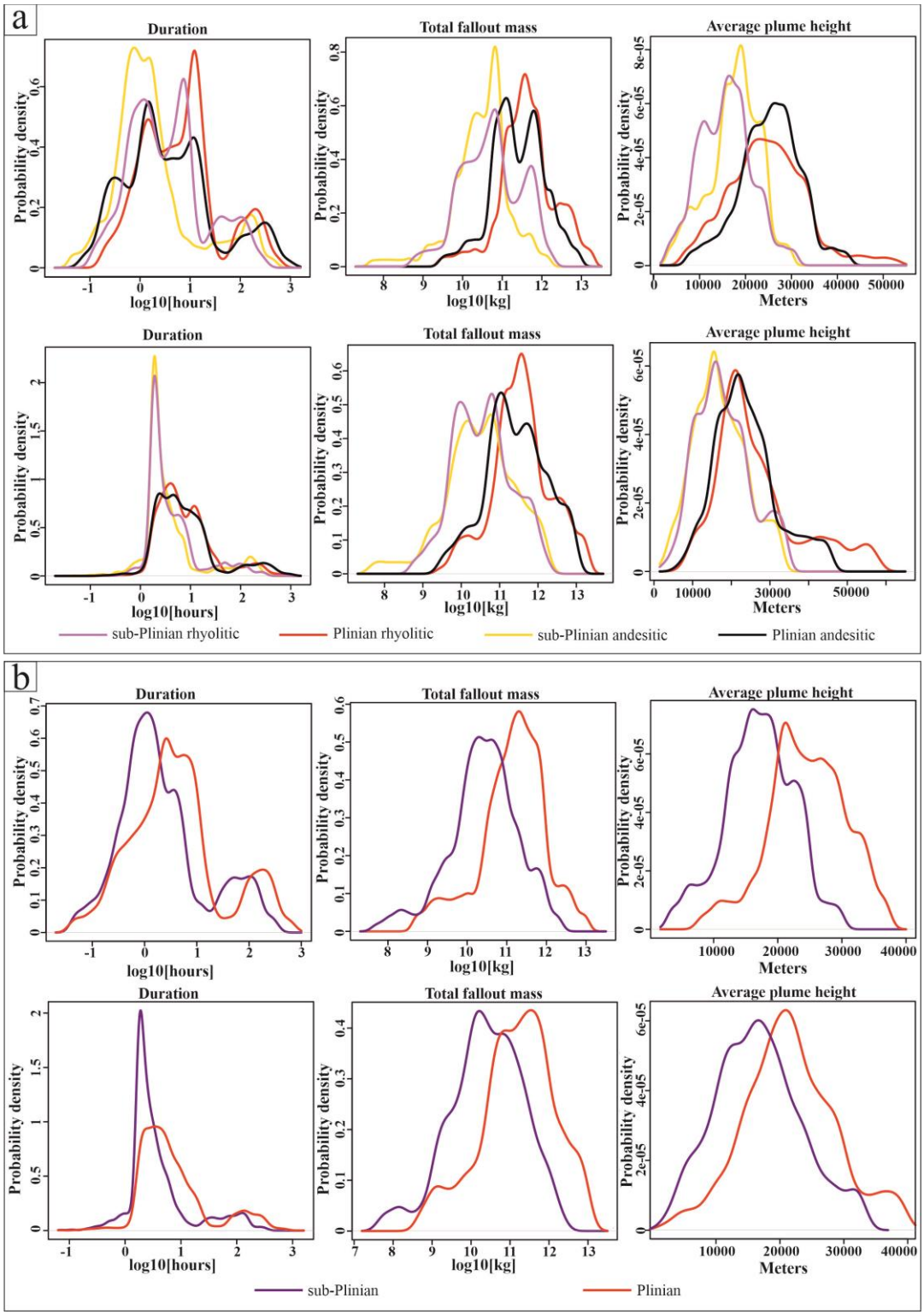


**Figure 3**. Eruptive source parameters (total eruption duration, total fallout mass and average plume height), uncertainty distributions according to the Classical Model method (from Tadini *et al.*, 2021; upper panels) and uncertainty distributions recalculated after the application of the relation of Mastin *et al.* (2009) (eqs. 2 and 3 - lower panels) for a) Cotopaxi and b) Guagua Pichincha volcanoes. y-axis describes the density of the probability density function.

For other parameters, such as total grain-size distribution (TGSD), particle densities, particle shape factors (i.e. sphericity), and initial volatile content of magma, we considered an uncertainty range variable between two end members. In detail, for particle density we considered that this parameter increases linearly between those typical of a coarser and a finer grain size end-members, according to Bonadonna & Phillips (2003). Uncertainty bounds for this latter parameter have been derived from Bonadonna & Phillips (2003) and Pistolesi *et al.* (2011). For TGSD, instead, we considered the relationship discussed in Costa *et al.* (2016a), who proposed that TGSD distributions (for each eruption and magma types) can be described by the sum of two log-normal distributions as a function of plume height and magma viscosity. Details of these relations are provided in the Appendix. In our study, we have considered TGSD in the range $\Phi$ = -6 to $\Phi$ = 10 (see Table 2 for the range of median and sorting of the total grain size distributions used in the simulations). Regarding the uncertainty ranges of the other parameters, we relied on the constraints given in literature for the pre-eruptive water contents for Cotopaxi and Tungurahua magmas (Andújar *et al.*, 2017; Martel *et al.*, 2018; Samaniego *et al.*, 2010; Wright *et al.*, 2007), and particle shape factors (Riley *et al.*, 2003) of other volcanoes. The complete list of the parameters (other than those reported in Table 2) is available in Table S3 from the supporting information.

For meteorological data, we have used those deriving from the GDAS forecast data (NOAA, 2004), covering the period December 2004 – December 2019. This meteorological dataset (tested by Tadini *et al.*, 2020) collects atmospheric data on 23 pressure levels (plus ground data) with a spatial grid resolution of 1° x 1° and a temporal resolution of 3 hours. An example of wind directions/velocities at a selected pressure level (200 hPa) above Cotopaxi volcano is provided in Figure S1 from the supporting information, which shows that main wind directions are toward NW/W/SW with the exceptions of December and January. Despite the availability of more spatially and temporally refined meteorological datasets (e.g. the ERA5 reanlysis dataset; Hersbach *et al.*, 2020), we have chosen the GDAS meteorological dataset for two reasons. Firstly, GDAS data can be directly read by HYSPLIT after their download without conversion and/or assemblages from separate files (as it is necessary for the ECMWF datasets like ERA-Interim or ERA5). This has the advantage of simplifying the procedure but also avoiding possible errors during the conversion procedure. Secondly, Tadini *et al.* (2020) showed that there is not a meteorological dataset that systematically provides better results (see Section 3.1.2), and the uncertainty of the model could be only partially be ascribed to the employment of one meteorological dataset compared to another. Future developments could include a deeper usage of the newly released datasets like the ERA5 in order to provide a comparison with the present results.

## 3.3 Hazard maps and curves

### 3.3.1 Parameters sampling and maps production

In order to explicitly quantify the different uncertainties, in this study we have implemented a new and comprehensive procedure for parameter sampling and map production, as illustrated in Fig. 4. This figure shows the procedure for each eruption type and for each iteration.

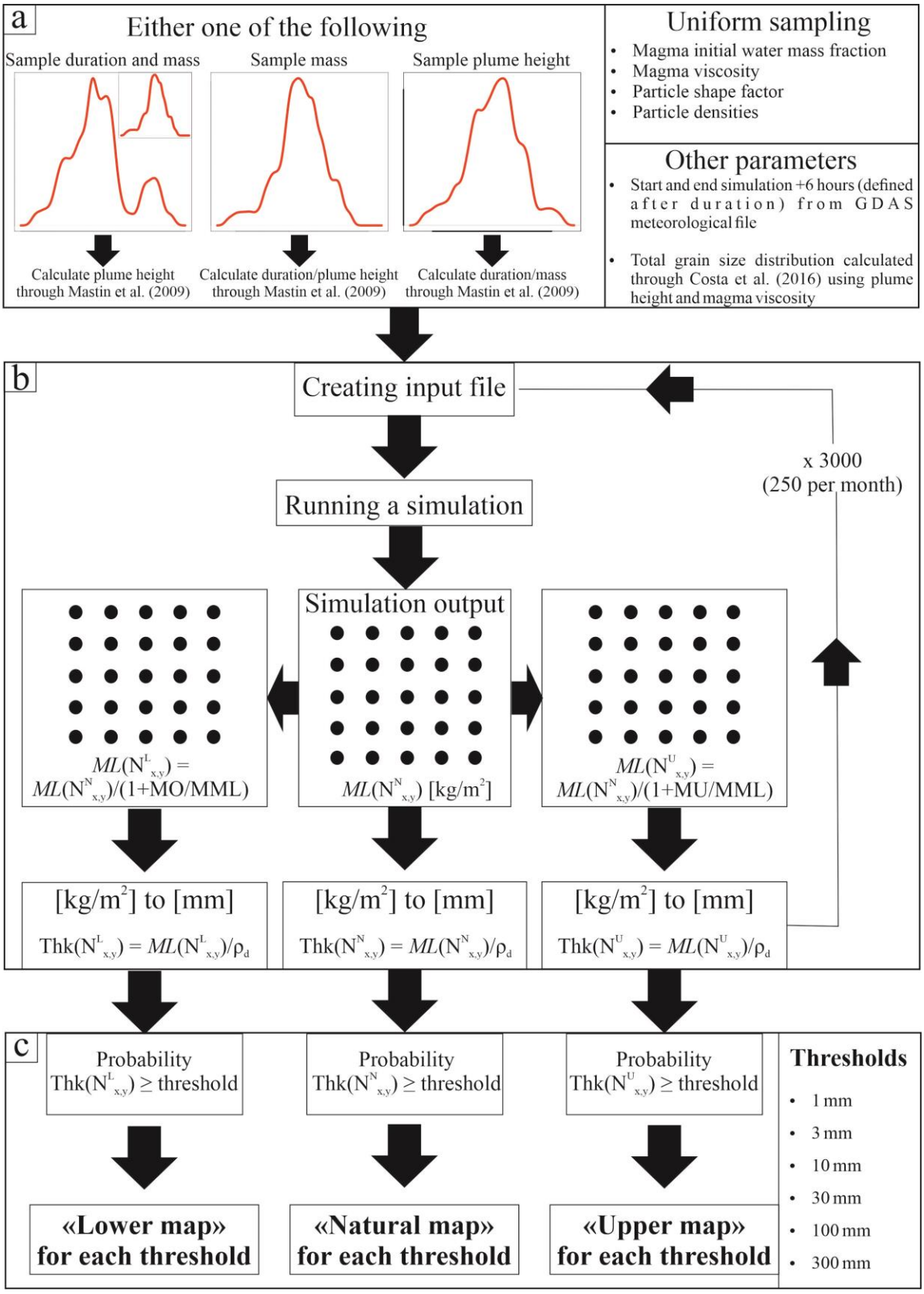
a
Either one of the following
Sample duration and mass
Sample mass
Sample plume height
Calculate plume height through Mastin et al. (2009)
Calculate duration/plume height through Mastin et al. (2009)
Calculate duration/mass through Mastin et al. (2009)
Uniform sampling
Magma initial water mass fraction
Magma viscosity
Particle shape factor
Particle densities
Other parameters
Start and end simulation +6 hours (defined after duration) from GDAS meteorological file
Total grain size distribution calculated through Costa et al. (2016) using plume height and magma viscosity
b
Creating input file
Running a simulation
Simulation output
x 3000
(250 per month)
ML(N^L_x,y) = ML(N^N_x,y)/(1+MO/MML)
ML(N^N_x,y) [kg/m²]
ML(N^U_x,y) = ML(N^N_x,y)/(1+MU/MML)
[kg/m²] to [mm]
Thk(N^L_x,y) = ML(N^L_x,y)/ρd
[kg/m²] to [mm]
Thk(N^N_x,y) = ML(N^N_x,y)/ρd
[kg/m²] to [mm]
Thk(N^U_x,y) = ML(N^U_x,y)/ρd
c
Probability Thk(N^L_x,y) ≥ threshold
Probability Thk(N^N_x,y) ≥ threshold
Probability Thk(N^U_x,y) ≥ threshold
«Lower map» for each threshold
«Natural map» for each threshold
«Upper map» for each threshold
Thresholds
1 mm
3 mm
10 mm
30 mm
100 mm
300 mm

435

**Figure 4**. Sketch of the procedure for map production. a) Parameter sampling for each iteration. Mass, duration and plume height are sampled from the elicited distributions and adjusted according to Mastin *et al.* (2009), while other parameters are sampled from uniform distributions and TGSD is sampled using the relation of Costa *et al.* (2016a); b) processing of simulations. A total of 3000 simulations for each eruption type (250 per month) are done. Each simulation output is corrected with the two coefficients that account for model uncertainty (MO/MML and MU/MML) and two additional maps are created. Mass loading values (ML) are then converted to thickness (Thk) using a mean value of deposit density ($\rho_d$); c) post processing and development of probability maps. For each map and each thickness threshold (1, 3, 10, 30, 100, 300 mm) it is evaluated the probability that, at each node of the map, Thk ≥ threshold. Three final maps are produced, "Natural", "Lower" and "Upper".

The uncertainty affecting the eruptive source parameters (ESPs) was taken into account with a Monte Carlo sampling (Fig. 4a). The three main ESPs (eruption duration, total mass of tephra fallout deposit, and average plume height) have been sampled directly from the distributions provided by Tadini *et al.* (2021) and reported in Fig. 3.

However, in order to avoid the use, within each simulation, of physically unrealistic combinations of parameters, we have considered the relations described in Mastin *et al.* (2009) that link plume height (in km) with volumetric flow rate (VFR in $m^3/s$) and total volume (V in $km^3$) of the fallout deposit, which are

$$H = 2.00 * VFR^{0.241} \quad (2)$$

$$H = 25.9 + 6.64 log_{10}(V) \quad (3)$$

Therefore, we have defined three possible cases, imposing that one third of the Monte Carlo iterations follows each case:

- total mass is sampled and duration/plume height are calculated (equations 2-3);
- plume height is sampled and total mass/duration are calculated (equations 2-3);
- duration and total mass are sampled and plume height is calculated (equation 2).

For the latter case, duration and total mass have been sampled independently due to the absence of a strong relationship between eruption duration and the other parameters (as also pointed out by Mastin *et al.*, 2009). In detail, the total mass of tephra fallout deposit (in kg) enabled the calculation of the mass flow rate (kg/s) using eruption duration. To convert our mass and mass flow rate to, respectively, volume and volumetric flow rate, we have used magma DRE densities and tabulated values from Spera (2000) of 2340, 2220 and 2110 $kg/m^3$ for, respectively, andesitic, dacitic and rhyolitic melts. Density values have been chosen corresponding to magma water contents compatible to the ranges used here (see Table S2 from the supporting information).This procedure has the advantage of creating set of parameters physically related for each simulation, although it introduces some alterations with respect to the original elicited values. We found these differences not significant, except for eruption duration (see Fig. 3), which reduced the probability of samples below 60 minutes, and thus had mean values slightly higher than the elicited one for all the eruption types. Conversely, when analyzing the contribution of the three above-mentioned cases in exploring the sample space, we noted that only method 3 (i.e. duration/total mass sampled and plume height calculated) captures the longest elicited durations (see Fig. S2 from the Supporting Information). Nevertheless, although this is significant to mention in terms of seeking future improvements of input parameters handling, the changes in duration do not significantly influence our hazard assessment because

they mostly affect the eruptions of the shortest duration and, in absolute terms, prolong them of a few tens of minutes. In general, since our study focuses on medium-large magnitude eruptions (i.e. VEI 3-4, sub-Plinian to Plinian), using the relations of Mastin *et al.* (2009) is appropriate in order to avoid the limitations of these relations themselves, which are less precise for small-size eruptions.

We highlight that PLUME-MoM cannot take at the same time mass flow rate and plume height as input parameters, and thus the plume height in our procedure (both sampled from the elicited distribution of Tadini *et al.*, 2021 or calculated after Mastin *et al.*, 2009) can be different with respect to the plume height calculated by PLUME-MoM by using the sampled total mass and duration. In case the elicited plume height is sampled (and therefore mass flow rate is calculated with Mastin *et al.*, 2009 and provided as input to PLUME-MoM), we found that PLUME-MoM can provide plume height values ~30-40% lower, at the end of simulation, with respect to those used to calculate the total mass/duration. This is perhaps related to the fact that the relation between plume height and mass flow rate of Mastin *et al.* (2009) is mostly based on maximum plume height values while the elicited plume heights arevalues averaged over the course of the eruption. However, the uncertainty bounds provided by Mastin *et al.* (2009) and the uncertainty range of our elicitation are fully overlapping and greater than the above-mentioned differences.

As previously mentioned, plume height and magma viscosity enabled us to calculate total grain-size distribution according to the relation proposed by Costa *et al.* (2016a) (see previous section, Appendix, and Table 2). However, differences in the TGSD due to the plume height discrepancy are not significant.

We finally remark that the duration of the eruption was also used to select (from the GDAS meteorological file covering the period 2004-2019) a time period for meteorological data. To this time period, additional 6 hours of simulation (with no emission) have been added to allow the particles to settle. To account for monthly variations in atmospheric data (see Figure S1 from the supporting information), we have performed the same number of simulations for each month (250, chosen as the best compromise between output accuracy and computation time). In total, we performed 3000 simulations for each eruption type.

The uncertainty due to the numerical model has been quantified during the processing of simulations (Fig. 4b). During this stage, the sampled parameters have been assembled to create an input file for the model, and at the end of the simulation an output in the form of a sampling grid has been provided, where each node $N^N_{x,y}$ (with x and y being latitude and longitude coordinates) has a mass loading value *ML* (in kg/m$^2$). By using the two coefficients MO/MML and MU/MML described in Tadini *et al.* (2020) and in section 3.1.2, two additional maps were created:

- a map with nodes $N^L_{x,y}$ that corrects model overestimation, such that $ML(N^L_{x,y}) = ML(N^N_{x,y})/(1 + MO/MML)$, where $MO/MML = 1.48$ is the coefficient of overestimation (see section 3.1.2);
- a map with nodes $N^U_{i,j}$ that corrects model underestimation, such that $ML(N^U_{x,y}) = ML(N^N_{x,y})/(1 + MU/MML)$ where $MU/MML = -0.49$ is the coefficient of underestimation (see section 3.1.2).

The mass loading values of each map (in kg/m$^2$) were then converted into thickness values (in mm) by dividing them with deposit density average values. For Cotopaxi we have used 825 kg/m$^3$ for andesitic (average among values used by Tsunematsu & Bonadonna, 2015) and 560 kg/m$^3$ for rhyolitic (Bonadonna *et al.*, 2015b) magmas. For Guagua Pichincha, given the general paucity of published data, we have collected 22 samples from tephra fallout deposits from both the X century (12 samples) and Historic (10 samples) eruption cycles (Figure S3 from the Supporting Information). The average value of the calculated deposit densities (measured as the ratio mass/volume of the 22 samples) yields an average value of 745 kg/m$^3$.

Once all simulations were finished, probabilistic maps were produced in a post-processing stage (Fig. 4c) following the approach of Bonadonna (2006). According to this latter, the probability $P_\tau$at each node $N_{x,y}^N$ (for the simulation output, same for $N_{x,y}^L$ and $N_{x,y}^U$) is determined by summing the number of times a certain thickness threshold (Thk) is reached and dividing it by the total number m of the simulations:

$$P_\tau\left(N_{x,y}^N\right) = \frac{\sum_{i=1}^{m} n_i}{m} \quad (4)$$

where

$$n_i = \begin{cases} 1, & if\ \left[Thk\left(N_{x,y}^N\right) \geq \tau\right] \\ 0, & otherwise \end{cases} \quad (5)$$

In this study we have used six different thresholds $\tau$ (in mm, Fig. 4c), chosen to be comparable with existing hazard maps and hazard-related studies. Three maps were in the end produced ("Lower", "Natural" and "Upper"), defining a set of maps that quantify the uncertainty associated with the model. This procedure has been applied for all the six eruption types considered in this study (see section 3.3.2).

### 3.3.2 Maps and curves format

We focused on medium to large magnitude eruptions, i.e. those with VEIs ≥ 3 corresponding to sub-Plinian to Plinian eruptive styles (i.e. those for which the model performs better). For the two studied volcanoes, this corresponds to four eruption types for Cotopaxi (sub-Plinian/Plinian with rhyolitic magmas, and sub-Plinian/Plinian with andesitic magmas) and two eruption types for Guagua Pichincha (sub-Plinian and Plinian with dacitic magmas). Different maps have therefore been produced for each eruption type and thickness threshold (see section 3.3.1). Moreover, for each volcano, the corresponding maps have been merged to produce a unique set of maps according to the procedure detailed in section 3.3.3. To limit the computational times, the computational domain of the simulations has been imposed equal to a square of 1.5°x1.5° centered on each volcano.

The resulting maps (produced through a post-processing procedure into the ArcGIS10© software) follow a format similar to those proposed by Biass & Bonadonna (2013), which are: i) probability maps (in which we are showing the 10% and 50% probability isolines) corresponding to a thickness threshold; and ii) isopach maps corresponding to a specific probability (10% and 50%). In addition, we derived hazard curves, which describe the probability of exceeding certain values of tephra accumulation at a given location (Bonadonna, 2006), at 10 sensitive sites within the city of Quito. These sites have been chosen because they could be heavily affected by tephra fall and could cause major issues to population and authorities. These sites are (Fig. 1a): Quito airport, Quito city center (UNESCO world heritage), Instituto Geofisico (IGEPN – Ecuador's

center for both volcanic and seismic monitoring), five hospitals, and two water treatment plants, all of them roughly distributed N-S along the city.

### 3.3.3 Merging of the maps

On top of the algorithm described in the previous section, we implemented an additional procedure that combines the scenarios of sub-Plinian and Plinian eruption types, weighted according to their probability of occurrence (Fig. 5). The uncertainty distributions of these probabilities have been estimated in Tadini *et al.* (2021) and are reported in Fig. 2a for Cotopaxi and Fig. 2b for Guagua Pichincha, for both the next eruption and the next 100 years cases. While the former is used in our merging procedure, the second is considered when analyzing the maps related to single eruption types in terms of a comprehensive hazard assessment of the next 100 years, and it is not used in this section.

In more detail, in case of two eruption types a and b (Fig. 5), for each thickness threshold, the procedure illustrated in section 3.3.1 provides two sets of three output maps (Lower, Natural and Upper). Each map is composed of a series of nodes ($N_{x,y}^{L}$, $N_{x,y}^{N}$ and $N_{x,y}^{U}$ for the Lower, Natural and Upper, respectively) that describe the probability *P* of exceeding a certain thickness. The goal of our merging procedure is to combine the probabilities of each node in each map (for our example, $P_{\tau}(N_{x,y}^{L,a})$ and $P_{\tau}(N_{x,y}^{L,b})$ for the Lower; same for Natural and Upper) according to the probabilities *P(a)* and *P(b)* that the next eruption will be either *a* or *b*. To do so, we initially sample *m*=1000 probabilities for each eruption type from the probability density functions of the corresponding eruption type of Fig. 2 (next eruption case), which are then normalized to sum to 100%. Such probabilities are then used to derive *m* map sets, where the probability of the node of each map is the result of a weighted mean with respect to *P(a) and P(b)*. In other words, for each node we derive a vector composed of *m* elements, each of them resulting from the weighted mean of the original probabilities. Finally, the set of three maps for each thickness threshold related to the next eruption (conditional to the occurrence of either eruption a or b) is obtained by sampling, from the vector of each node of the grid:

- for the final Lower map, the $5^{th}$ percentile of the distribution of the vector;
- for the final Natural map, the mean (*E*) of the distribution of the vector;
- for the final Upper map, the $95^{th}$ percentile of the distribution of the vector.

In this way we are able to show the full extent of the uncertainty linked to different eruption types (given by the $5^{th}$ and $95^{th}$ percentiles), with a mean value that ultimately represents the actual outputs of the model for each eruption type combined with mean values of eruption occurrences.

As already discussed, this merging procedure has been applied to combine four eruption types of Cotopaxi volcano (sub-Plinian andesitic/rhyolitic and Plinian rhyolitic/andesitic) and two eruption types for Guagua Pichincha volcano (sub-Plinian and Plinian). The same procedure has been used to combine the hazard curves of all the 10 sites.

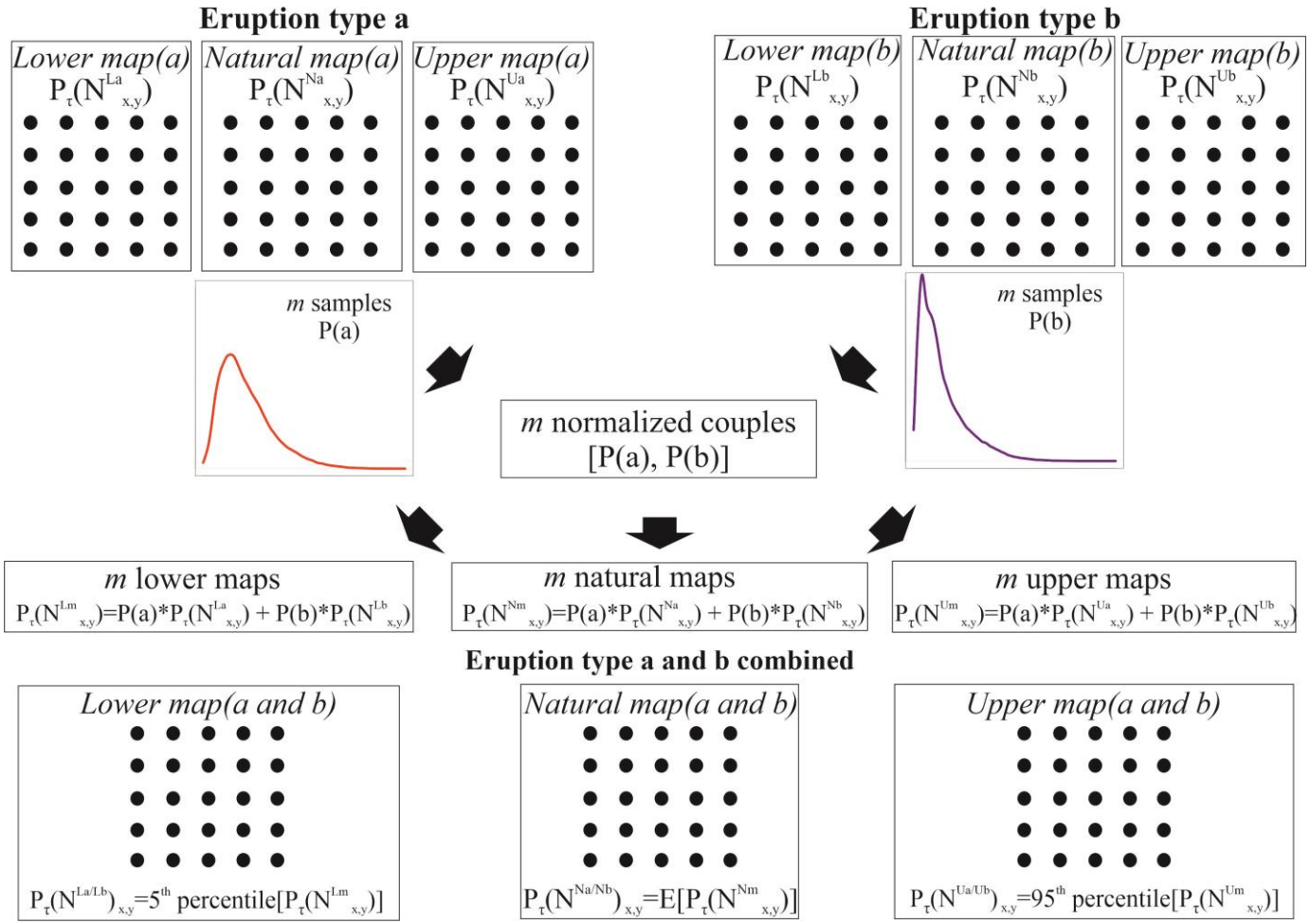


**Figure 5**. Sketch illustrating the procedure used for merging the set of maps of two eruption types (a and b). Two eruption types a and b have, each of them, a set of three maps (Lower/Natural/Upper). From the distribution of probability of Fig. 2 (next eruption case) two probabilities (one per distribution) are sampled and then normalized. For each map type, the probability at each node for the combined a and b is calculated as the weighted mean (using the two normalized values) of the original two maps. This procedure is performed for m=1000 times, yielding (for each node of each map type) a vector of 1000 probability values. Finally, from each vector is extracted the value corresponding to, respectively, the 5$^{th}$ percentile (for the Lower map) the mean (for the Natural map) and the 95$^{th}$ percentile (for the Upper map) of the vector.

# 4 Results and discussion

In the following sub-sections, we present and discuss separately the merged probabilistic and isopach maps and the hazard curves for both Cotopaxi (Figs. 6-8) and Guagua Pichincha (Figs. 9-11) volcanoes. In order to simplify the results (see section 3.3.2), for probability maps we plotted a colored band between upper and lower isolines that highlights both the effects of the uncertainties of the numerical model (see section 3.3.1) and in the probabilities of occurrence of the different eruption types considered see section 3.3.3). Instead, for isopach maps we show only the upper isolines to present the worst result in a conservative approach. We also report, in Tables 3-4, the areal extent covered and the population potentially affected by single isopach lines corresponding to 10% and 50% probabilities for both volcanoes. We remark that this is not a risk quantification, which would require a vulnerability assessment that is not the focus of this paper. For the population potentially affected, we have used data from the LandScan database (Rose *et al.*, 2020). We stress that some isolines extend further out of the computational domain, and therefore the areas and the population potentially affected represent minimum estimates. Additionally, we include in the supporting information the maps/curves for each single eruption type (Figs. S4-S57) and the calculated exceeding probability values for each accumulation threshold, each eruption type and each sensitive site related to the hazard curves (Table S4). Our results follow a "doubly stochastic" approach, made of two stages.First, we varied the ESPs to produce "classical" hazard maps and curves, and secondly we evaluated the effects of the uncertainties affecting both numerical model and eruption type probability of occurrence. Similar procedures have been applied in pyroclastic density current hazard assessments (Bevilacqua *et al.*, 2017, 2021; Neri *et al.*, 2015; Rutarindwa *et al.*, 2019), but not in the case of an ash fallout hazard assessment. In addition, previous studies did not evaluate the effects of the model uncertainty on the hazard assessments systematically. We remark that our uncertainty assessment highlights how large the uncertainty is, implying that the current knowledge of tephra fallout dispersion and deposition does not allow us to accept or reject previous hazard maps. Those maps are in fact mostly enveloped by our assessments but represent a less complete hazard evaluation because they do not consider all the uncertainty sources that we modeled. Our results show that presenting a single volcanic hazard map for a specific eruption probability, would provide an incomplete volcanic hazard assessment. Conversely, presenting a comprehensive set of hazard maps related to the uncertain probabilities of one or more eruption types fully pictures the current available knowledge. If our three maps, i.e. the $5^{th}$ percentile, the mean, and the $95^{th}$ percentile values, are considered too complex to be presented to a general audience and/or to be used by the authorities, then only one of them could be used as a reasonable statistical summary after a discussion with stakeholders and decision-makers. However, this choice would hide some of the uncertainty to the audience.

## 4.1 Cotopaxi

At Cotopaxi, the amount of people potentially affected (especially considering the 50% isolines, see Table 3) is considerable (Figs. 6-7), since seven cities/towns are potentially affected by tephra fall accumulations. Among them, three have > 100,000 inhabitants (Quito, Ambato and Santo Domingo), one has > 25,000 (Latacunga), two have > 5,000 (Machachi and Tena) and one has < 5,000 (Baeza). A striking feature of the maps presented is the drastic changes in people potentially affected within the Lower-Natural-Upper maps.

Considering for instance the 10% isolines (Table 3), for the 10 mm isopach the people potentially affected change from 313,000 (Lower) to more than 4 million (Upper). Concerning the maps themselves, the prevailing winds toward W imply that areas in this direction have higher probabilities of tephra accumulation, which could potentially cause severe issues for both building stability and infrastructures, such as the "Pan-American" highway (see Figs. 6-7 and also Biass & Bonadonna, 2013).

Table 3 can be used for a partial comparison with the work of Biass & Bonadonna (2013), with which our paper shares similarities in the modelling strategy and product outputs, although these authors did not consider the uncertainties in the eruption type probabilities and in the numerical model results. With respect to the areas covered by their 1, 10, 100, 300 kg/m$^2$ (roughly comparable to our thickness thresholds) for the 50% probability, our estimated areas are generally in agreement with theirs. For example, in Biass & Bonadonna (2013) the area covered by the 1 kg/m$^2$ isomass for an eruption scenario VEI 3-5 for the next 100 years is 7,900 km$^2$, while in our Upper (95$^{th}$ percentile) map, the area covered by the 1 mm isopach is 8,777 km$^2$ (Table 3). The comparison between our results and those in Biass & Bonadonna (2013) is however complicated by the many methodological differences in i) the model employed, ii) the use of thickness thresholds, iii) the consideration of eruption types rather than single VEIs, and iv) the choice of focusing on the next eruption rather than the next 100 years for combined eruption types (with differences in the estimation of probabilities of occurrence). Nevertheless, further improving the consistency between the elicited values of plume height, the empirical correlation formulas, and the numerical simulator output, within a fully fledged uncertainty assessment is a compelling task for additional research.

Considering the impact of tephra accumulation on airports, our maps indicate that two to four airports could be affected by a tephra accumulation of 1 mm with a probability of at least 10% (see Figs. 6 and 7). Among them, Quito international airport (Fig. 8) could have a tephra accumulation of 1 mm and 10 mm of, respectively, 6-27% and 1-14% (Table S4 from the Supporting Information). Such values are in agreement with those proposed by Volentik & Houghton (2015), who calculated the same probabilities as, respectively, 14-20% and 2.5-6%.

Bebbington *et al.* (2008) estimated that an accumulation of 1-2 mm of ash could be sufficient for flashovers to occur along the normal electrical networks, and therefore to cause voltage fluctuations and power shutdown, as also shown by López *et al.* (2016) for Cotopaxi and Tungurahua volcanoes. For Cotopaxi, this accumulation could concern three to five power plants and 329 to 626 km of the electrical network, if we consider, respectively, the lower and upper 10% probability contours (Figs. 6-7).

Concerning the sensitive sites in Quito (Figs. 1a and 8), the probabilities for an accumulation of 10 mm (an average of the accumulation thresholds chosen) could be 3-23% for Quito city center (with possible consequences on the cultural heritage), 2-19% for IG-EPN Quito (with possible impact on instrumentation and data transmission systems for volcanic and seismic monitoring), 1-27% for the five hospitals chosen (with possible problems on ventilation and power supply) and 2-20% for the water treatment plants (implying a possible contamination on water supply for the communities).

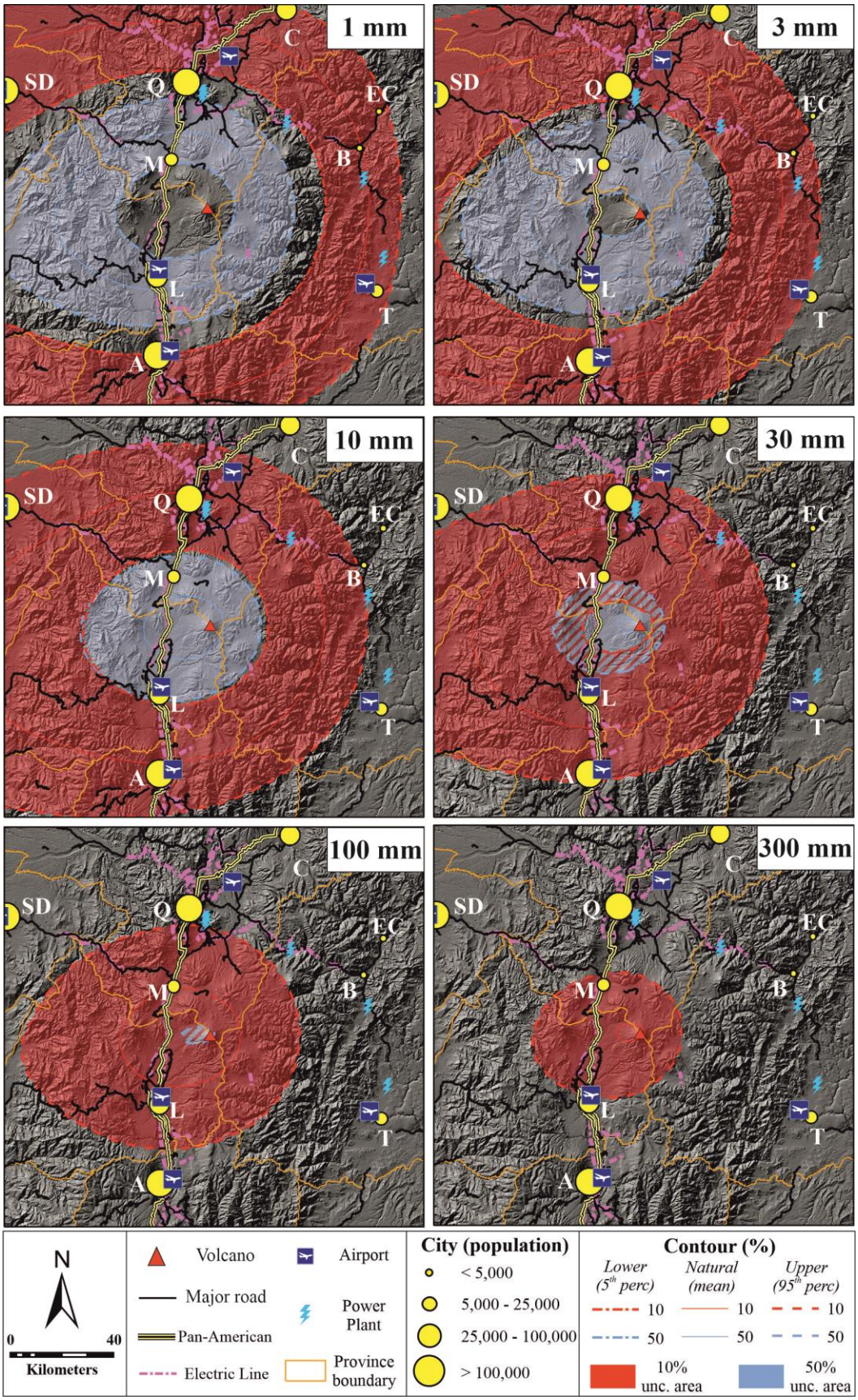
1 mm
3 mm
10 mm
30 mm
100 mm
300 mm
SD
Q
C
EC
B
M
L
T
A
N
0
40
Kilometers
Volcano
Airport
Major road
Power Plant
Pan-American
Electric Line
Province boundary
City (population)
< 5,000
5,000 - 25,000
25,000 - 100,000
> 100,000
Contour (%)
Lower (5th perc)
Natural (mean)
Upper (95th perc)
10
50
10% unc. area
50% unc. area

**Figure 6**: Probability maps (Cotopaxi volcano, red triangle) for different thickness accumulations in case the next eruption is sub-Plinian or Plinian. Uppercase letters are city names: A = Ambato, T = Tena, L =Latacunga, M = Machachi, B = Baeza, SD =Santo Domingo, Q =Quito, EC = El Chaco, C = Cayambe. The extent of the maps is the same as the light blue dashed box of Fig. 1a. Digital Elevation Model (30 m- resolution) from Marc Souris, IRD.

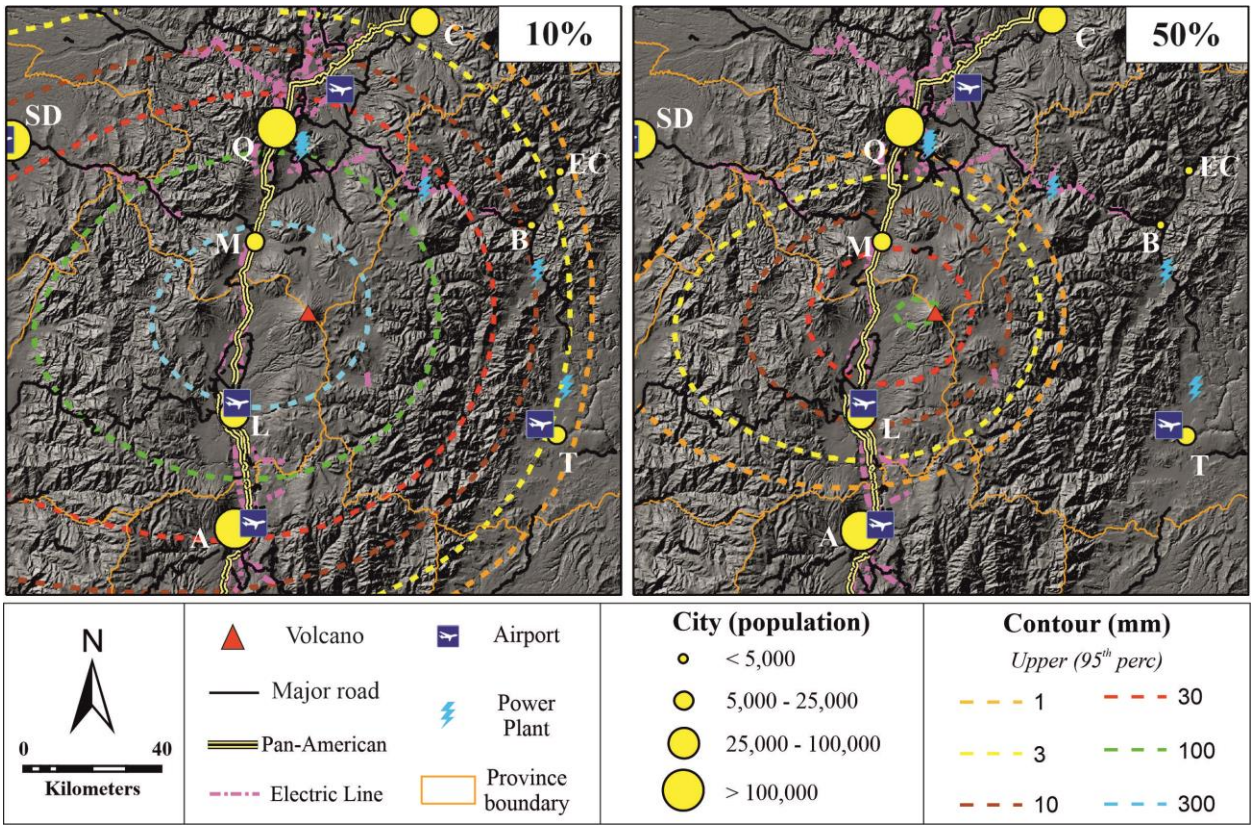


**Figure 7**: Isopach maps (Cotopaxi volcano, red triangle) for different probabilities in case the next eruption is sub-Plinian or Plinian. Uppercase letters are city names: A = Ambato, T = Tena, L =Latacunga, M = Machachi, B = Baeza, SD =Santo Domingo, Q =Quito, EC = El Chaco, C = Cayambe. The extent of the maps is the same as the light blue dashed box of Fig. 1a. Digital Elevation Model (30 m- resolution) from Marc Souris, IRD.

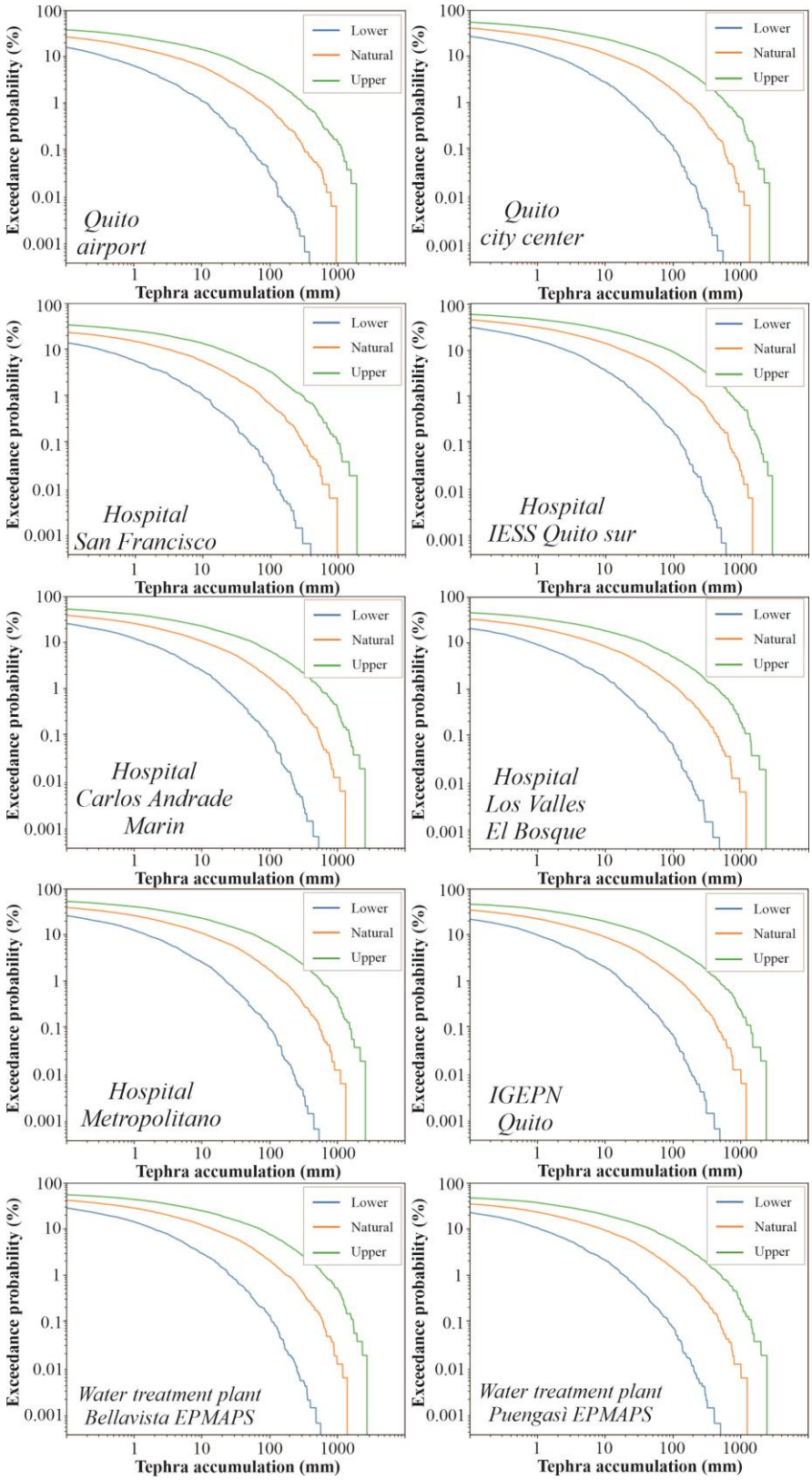


**Figure 8**. Hazard curves for 10 sensitive sites in Quito in case the next eruption at Cotopaxi is sub-Plinian or Plinian.

| Thickness (mm) | **Cotopaxi 10% probability** *Area Covered ($km^2$)* | | | **Cotopaxi 10% probability** *Population potentially affected* | | |
|---|---|---|---|---|---|---|
| | *Lower ($5^{th}$ perc)* | *Natural (Mean)* | *Upper ($95^{th}$ perc)* | *Lower ($5^{th}$ perc)* | *Natural (Mean)* | *Upper ($95^{th}$ perc)* |
| 1 | 12,779* | 20,444* | 25,159* | 2,226,274* | 4,092,923* | 4,390,708* |
| 3 | 8,495 | 16,504* | 23,257* | 1,199,996 | 3,729,036* | 4,234,693* |
| 10 | 3,649 | 11,615* | 19,080* | 313,436 | 1,987,021* | 4,063,216* |
| 30 | 453 | 6,348 | 14,058* | 16,041 | 640,204 | 2,794,615* |
| 100 | - | 1,511 | 7,822 | - | 101,884 | 1,130,590 |
| 300 | - | 58 | 2,411 | - | 28 | 183,065 |
| **Thickness (mm)** | **Cotopaxi 50% probability** *Area Covered ($km^2$)* | | | **Cotopaxi 50% probability** *Population potentially affected* | | |
| | *Lower ($5^{th}$ perc)* | *Natural (Mean)* | *Upper ($95^{th}$ perc)* | *Lower ($5^{th}$ perc)* | *Natural (Mean)* | *Upper ($95^{th}$ perc)* |
| 1 | 1,463 | 4,230 | 8,777* | 99,641 | 355,539 | 1,103,244* |
| 3 | 348 | 2,316 | 6,095 | 11,204 | 172,887 | 509,009 |
| 10 | - | 650 | 3,346 | - | 33,819 | 294,944 |
| 30 | - | 37 | 1,303 | - | 8 | 82,589 |
| 100 | - | - | 70 | - | - | 41 |

**Table 3**. Area covered and population potentially affected by tephra falls characterized by isopach contours corresponding to 10% and 50% probabilities for next sub-Plinian/Plinian eruption at Cotopaxi volcano. Numbers with * indicate that the corresponding isopach extends out of the computational domain, and the number itself is therefore an underestimation.

### 4.2 Guagua Pichincha

For Guagua Pichincha volcano, due to the proximity with the highly populated city of Quito, a small variation in the location of an isoline can change significantly the amount of people potentially affected. For example, for the 30 mm isopach line with 10% probability (Figs. 9-10), the change in the area covered given by the Lower ($5^{th}$ percentile) and Natural (Mean) maps is roughly 4,300 $km^2$ (from ~300 to ~4,600 $km^2$; Table 4), but the amount of people potentially involved changes from 425 to more than 2.7 million. Similar effects are evident also for the 100 mm (10% probability) and 3-10 mm (50% probability). We remark that previously existing hazard maps for Guagua Pichincha (see section 2.2) were only semi-probabilistic, thus the comparison with our results is difficult. However, we note that our maps appear to have smaller isoline areas, on average, than the previously mentioned assessments. The drastic change in people potentially affected is also linked to the fact that the main direction of wind blowing is toward W (see Figure S1 from the supporting information). This is consequently the main direction of isolines elongation, and since the amount of people living in this area is low (due to the presence of the rain forest), the small upwind changes of isoline areas to the E (where Quito is located) are the major causes for the drastic changes in the population potentially affected. It is

760 however important to highlight that the spatial resolution of the meteorological dataset used
761 plays a role in these situations, since different resolutions could cause fluctuations in the position
762 of the isoline resulting in important variations in the population affected. In this study, we have
763 chosen a meteorological dataset that optimized the simulation process, but future developments
764 could consider more refined metorological datasets for highly critical areas where it is required
765 an higher degree of accuracy. In general, considering all the isolines and their uncertainties, eight
766 cities/towns might experience different degrees of tephra fall accumulation, three of which with
767 > 100,000 inhabitants (Quito, Ibarra and Santo Domingo), three with > 25,000 (Latacunga,
768 Cayambe and Otavalo), one with > 5,000 (Machachi) and one with < 5,000 (Puerto Quito).
769 The uncertainty illustrated by the Lower-Natural-Upper maps is also particularly evident
770 with respect to the airports potentially involved. If we focus for example on the 1 mm isopach,
771 only two airports are included within the Lower ($5^{th}$ percentile) 10% isopach, while four are
772 included if we consider the Upper ($95^{th}$ percentile) 10%. For comparison, the Vulcanian 1999
773 eruption of Guagua Pichincha volcano caused an accumulation of 3-5 mm of ash within the old
774 location of Quito airport, and the subsequent closure of the airport for eight days (Guffanti *et al.*,
775 2009). Concerning the new Quito airport, our study provides a specific hazard curve for this site
776 (Fig. 11) with exceeding probabilities (Table S4 from the supporting information). Our
777 probabilities for the 1 mm (25-54%) and 1 cm (7-33%) accumulation are higher than those
778 provided by Volentik & Houghton (2015) (17-20% and 7-8% for the 1 mm and 1 cm,
779 respectively). This is due to the different range of parameters used and the different models
780 employed.
781 Considering the already mentioned threshold of 1-2 mm of ash that could cause electrical
782 flashovers (Bebbington *et al.*, 2008; López *et al.*, 2016) and the maps of Fig. 10, two power
783 plants have 50% probability to have accumulation of 1-3 mm, while another one has 10%
784 probability for the same accumulation. Electric lines concerned by an accumulation of 1 mm are
785 at least 416 to 542 km long considering, respectively, the lower and upper isoline of the 10%
786 (Fig. 9) For comparison, during the 1999 eruption of Guagua Pichincha that caused < 5 mm
787 accumulation of ash in Quito, the local thermal power stations stopped their activity as a
788 precautionary measure (d'Ercole & Metzger, 2000).
789 Specifically for the city of Quito, a sub-Plinian to Plinian eruption could lead to ash
790 accumulation of 1 cm with probabilities for the analyzed sites (Figs. 1a and 11 and Table S4
791 from the supporting information) of i) 13-49% for the five hospitals, ii) 17-58% for city center,
792 iii) 14-50% for IGEPN Quito and iv) 15-57% for the two water treatment plants. With respect to
793 the latter, we recall that, during the 1999 eruption of Guagua Pichincha, a treatment plant in
794 Quito had to be closed due to possible water contamination (d'Ercole & Metzger, 2000).
795

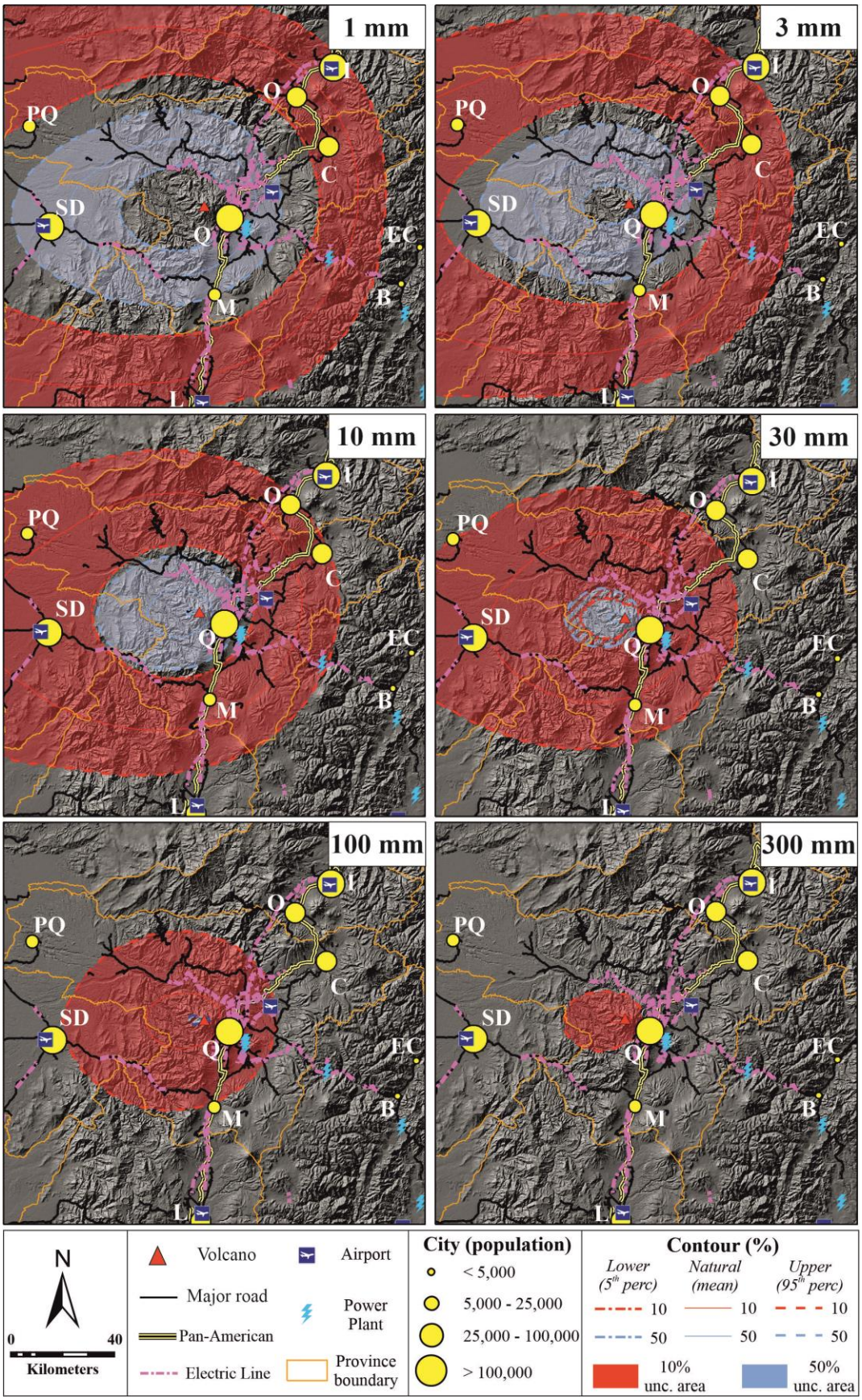
1 mm
3 mm
10 mm
30 mm
100 mm
300 mm
PQ
I
O
C
SD
Q
EC
B
M
L
N
0
40
Kilometers
Volcano
Airport
Major road
Power Plant
Pan-American
Electric Line
Province boundary
City (population)
< 5,000
5,000 - 25,000
25,000 - 100,000
> 100,000
Contour (%)
Lower (5th perc)
Natural (mean)
Upper (95th perc)
10
50
10% unc. area
50% unc. area

796

**Figure 9**: Probability maps (Guagua Pichincha volcano, red triangle) for different thickness accumulations in case the next eruption is sub-Plinian or Plinian. Uppercase letters are city names: L = Latacunga, M = Machachi, B = Baeza, SD = Santo Domingo, Q = Quito, EC = El Chaco, C = Cayambe, PQ = Puerto Quito, O = Otavalo, I = Ibarra. The extent of the maps is the same as the light green dashed box of Fig. 1a. Digital Elevation Model (30 m- resolution) from Marc Souris, IRD.

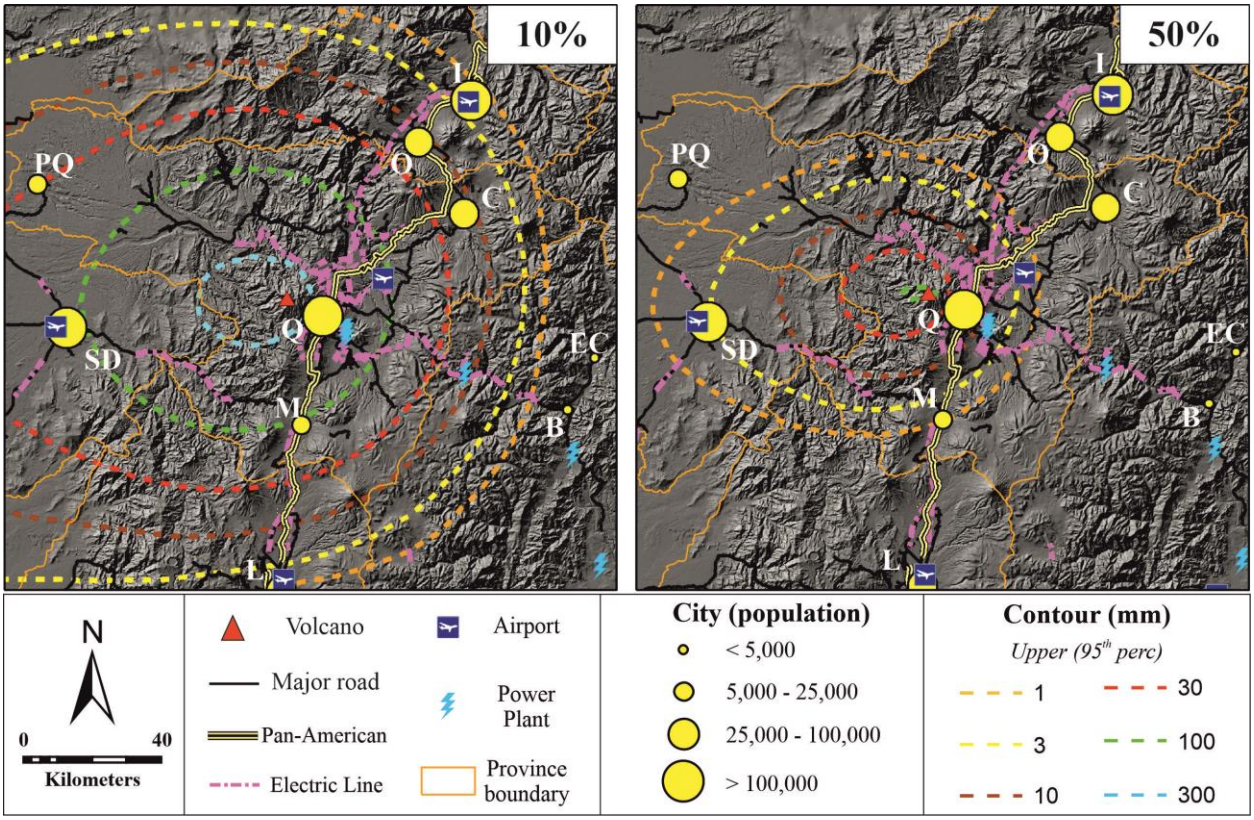


**Figure 10**: Isopach maps (Guagua Pichincha volcano, red triangle) for different probabilities in case the next eruption is sub-Plinian or Plinian. Uppercase letters are city names: L =Latacunga, M = Machachi, B = Baeza, SD = Santo Domingo, Q = Quito, EC = El Chaco, C = Cayambe, PQ = Puerto Quito, O = Otavalo, I = Ibarra. The extent of the maps is the same as the light green dashed box of Fig. 1a. Digital Elevation Model (30 m- resolution) from Marc Souris, IRD.

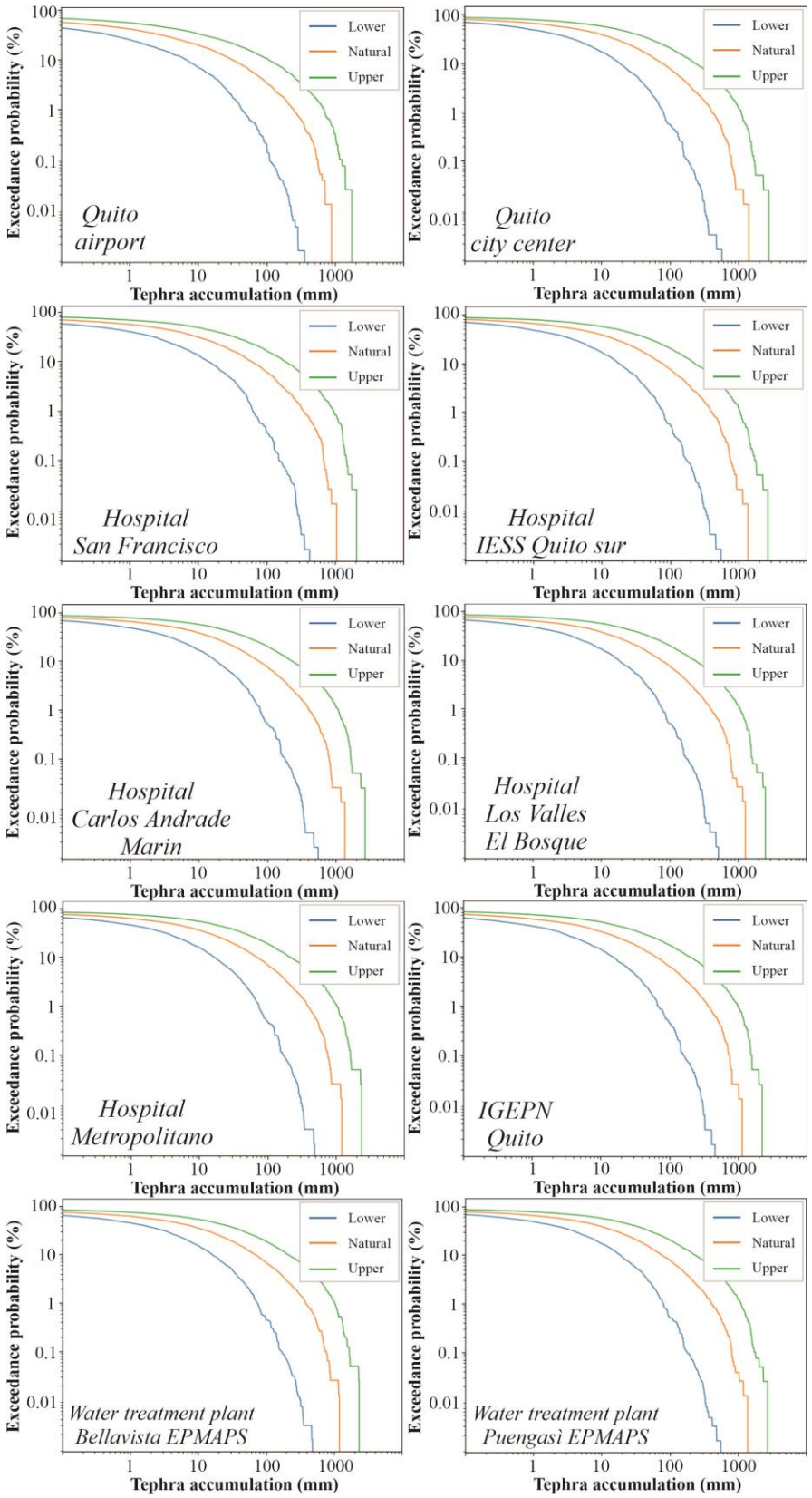


811
812 **Figure 11**. Hazard curves for 10 sensitive sites in Quito in case the next eruption at Guagua
813 Pichincha is sub-Plinian or Plinian.

| Thickness (mm) | **Guagua Pichincha 10% probability** *Area Covered ($km^2$)* | | | **Guagua Pichincha 10% probability** *Population potentially affected* | | |
|---|---|---|---|---|---|---|
| | *Lower ($5^{th}$ perc)* | *Natural (Mean)* | *Upper ($95^{th}$ perc)* | *Lower ($5^{th}$ perc)* | *Natural (Mean)* | *Upper ($95^{th}$ perc)* |
| 1 | 11,738* | 18,683* | 23,817* | 3,353,093* | 3,777,905* | 4,135,175* |
| 3 | 7,531 | 14,791* | 21,144* | 3,233,957 | 3,480,078* | 3,893,651* |
| 10 | 2,971 | 9,862* | 16,483* | 2,364,324 | 3,307,296* | 3,664,184* |
| 30 | 311 | 4,678 | 11,621* | 425 | 2,705,155 | 3,350,045* |
| 100 | - | 571 | 5,229 | - | 1,502 | 2,739,530 |
| 300 | - | 26 | 657 | - | 22 | 2,213 |
| **Thickness (mm)** | **Guagua Pichincha 50% probability** *Area Covered ($km^2$)* | | | **Guagua Pichincha 50% probability** *Population potentially affected* | | |
| | *Lower ($5^{th}$ perc)* | *Natural (Mean)* | *Upper ($95^{th}$ perc)* | *Lower ($5^{th}$ perc)* | *Natural (Mean)* | *Upper ($95^{th}$ perc)* |
| 1 | 1,249 | 3,368 | 6,955 | 152,655 | 2,285,577 | 3,145,383 |
| 3 | 315 | 1,757 | 4,538 | 387 | 1,506,818 | 2,690,885 |
| 10 | 8 | 417 | 2,225 | 4 | 925 | 1,886,192 |
| 30 | - | 25 | 605 | - | 21 | 1,552 |
| 100 | - | - | 26 | - | - | 19 |

**Table 4**. Area covered and population potentially affected by tephra falls characterized by isopach contours corresponding to 10% and 50% probabilities for next sub-Plinian/Plinian eruption at Guagua Pichincha volcano. Numbers with * indicate that the corresponding isopach extends out of the computational domain, and the number itself is therefore an underestimation.

## 5 Conclusions

This paper presents a tephra fallout hazard assessment for Cotopaxi and Guagua Pichincha volcanoes as well as an evaluation of the exposure of different sites and infrastructures in the region, with a specific focus on the consequences for the city of Quito. The results include probabilistic maps (for a fixed tephra accumulation and a fixed probability) and hazard curves for 10 sensitive sites in the city of Quito (airport, hospitals, city center, Instituto Geofìsico, water treatment plants), related to the specific case that the next eruption at both volcanoes could be either sub-Plinian or Plinian (VEI 3-5). Our new uncertainty quantification procedure has introduced, for all the eruption types and for both volcanoes, set of maps in which each isoline produced from the model output ("Natural") is corrected by producing two additional isolines that take into account model underestimation ("Upper") and overestimation ("Lower"). Our approach is relatively simple and straightforward, and we acknowledge that more studies are needed to refine the definition of the coefficients we used. For example, the tendency of the model to overestimate is greater than its tendency to underestimate, but this is mostly due to the overestimation of the model along the main dispersal axis: future studies could be possibly devoted to find a weighting scheme in the definition of the mean overestimation/underestimation that takes into account this tendency. For both volcanoes, the impacted area, the population and

the sensitive sites affected could vary significantly if these three isolines are considered. While some sources of uncertainty could be reduced due better-constrained the input parameters and by improving the modelling features of PLUME-MoM/HYSPLIT, we chose to show the current capabilities of the model by considering the model uncertainty in its widest range (i.e. considering correction coefficients from the worst simulated test eruption). Apart from hazard implications discussed in the previous sections, in our study:

- we have employed a coupling between a plume model (PLUME-MoM) and a tephra transport and dispersal model (HYSPLIT). HYSPLIT is currently used by several Volcanic Ash Advisory Centers (VAACs) and, to the best of our knowledge, has never been used so far to produce isopach tephra fallout hazard maps. Further employments of HYSPLIT for hazard maps production are advisable in order to find solutions for reducing its computational times and therefore considering larger computational domains and/or more refined computational grids. In this work, we have employed the GDAS meteorological dataset, with a spatial resolution of 1°x1° and a temporal resolution of 3 hours. While differences in the final results (i.e. hazard maps) could be only partial if another meteorological dataset was used (due to the many other sources of uncertainty detailed in this study), future developments could also take advantage of more recently released databases (e.g. ERA5), especially for critical areas where even a small shift in the position of an isoline could cause important consequences (see below);
- as sampling strategy, we chose to derive (for each eruption) sets of eruptive source parameters (duration, total mass of tephra fallout and plume height) physically consistent with real eruptions. We used the relations of Mastin *et al.* (2009) to calculate from one (or two) parameter(s) sampled the remaining two (or one). This procedure introduced correlations between the ESPs, but, as shown in section 3.3.1, also introduced some variations in the original sampling distributions. While such new distributions are within physically coherent ranges, other existing relations (e.g., Sparks *et al.*, 1997) could be employed to evaluate their effect on this recalculation.
- We performed the uncertainty quantification in two stages. First, by varying eruptive source parameters to produce "classical" hazard maps and curves, and then evaluating the effects of the uncertainties affecting both numerical model and eruption type probability of occurrence. This "doubly stochastic" approach increases the complexity of the final products, but the effects of the considered sources of uncertainty are significant and should not be averaged or neglected. In fact, even small shifts in the position of isolines can imply a significant change in the amount of people potentially affected by a given tephra accumulation, which has a direct implication in both emergency and long-term planning.

## Appendix: total grain-size distribution

Following Costa *et al.* (2016a), the total-grain size distribution is here considered to be composed of two log-normal distributions (i.e. Gaussian in Φ scale) with the form

$$f_{bi-Gauss}(\Phi) = \mathrm{p}\,\frac{1}{\sigma_1\sqrt{2\pi}}exp\left[-\frac{(\Phi-\mu_1)}{2{\sigma_1}^2}\right] + (1-p)\,\frac{1}{\sigma_2\sqrt{2\pi}}exp\left[-\frac{(\Phi-\mu_2)}{2{\sigma_2}^2}\right] \quad (6)$$

where $\mu_1$, $\mu_2$ and $\sigma_1$, $\sigma_2$ are respectively the mean and standard deviations of the two Gaussian distributions in distributions in Φ units, while p is the weight of each sub-population. Empirical

values to calculate these parameters have been proposed by the same authors and have been adapted to our study in the following form

$$\sigma_1 \approx 0.67 + 0.07\,H$$

$$\mu_1 + 3\sigma_1 \approx 0.96 + 0.20H$$

$$\mu_2 - \mu_1 \approx 1.62(Log_{10}\eta)^{0.66}$$

$$\sigma_2 \approx 1.46$$

$$p = 1.61\exp(-0.31Log_{10}\eta)$$

with H the plume height (km) and $\eta$ the magma dynamic viscosity (Pa s).

## Acknowledgments

The simulations have been performed on the cluster of the Laboratoire de Mathématiques Blaise Pascal and on the supercomputer facilities of the Mésocentre at Université Clermont Auvergne. We thank Damien Ferney for technical assistance, two anonymous reviewers for their constructive comments that improved the quality of the manuscript, an anonymous Associate Editor, and Editor in chief Isabelle Manighetti for editorial handling. This research was financed by the French government IDEX-ISITE initiative 16-IDEX-0001 (CAP 20-25), the French Research Institute for Sustainable Development (IRD) in the context of the Laboratoire Mixte International "Séismes et Volcans dans les Andes du Nord" (collaboration between IG-EPN Quito and LMV Clermont-Ferrand), and the CNRS Tellus programme. This work was also partly funded by the ClerVolc project - Programme 1 "Detection and characterization of volcanic plumes and ash clouds" funded by the French government 'Laboratory of Excellence' initiative. This is Clervolc contribution number XXX.
The authors have no competing interests to declare.
Data supporting the analyses and conclusions presented in this study could be found in a repository in the Figshare community with the following DOI: https://figshare.com/s/d039d9c741040b70c88c

## References

Alpízar Segura, Y., M. Fernández Arce, C. Ramírez Umaña, & D. Arroyo Alpízar (2019), Hazard Map of Rincón de la Vieja Volcano, Costa Rica: Qualitative Integration of Computer Simulations and Geological Data, *Anuario do Instituto de Geociencias*, *42*(3), doi:http://dx.doi.org/10.11137/2019_3_474_488.

Andújar, J., C. Martel, M. Pichavant, P. Samaniego, B. Scaillet, & I. Molina (2017), Structure of the plumbing system at Tungurahua volcano, Ecuador: insights from phase equilibrium experiments on July–August 2006 eruption products, *Journal of Petrology*, *58*(7), 1249-1278, doi:https://doi.org/10.1093/petrology/egx054.

Annen, C., & J. J. Wagner (2003), The impact of volcanic eruptions during the 1990s, *Natural Hazards Review*, *4*(4), 169-175, doi:https://doi.org/10.1061/(ASCE)1527-6988(2003)4:4(169).

Armienti, P., G. Macedonio, & M. T. Pareschi (1988), A numerical model for simulation of tephra transport and deposition: Applications to May 18, 1980, Mount St. Helens eruption, *Journal of Geophysical Research: Solid Earth*, *93*(B6), 6463-6476, doi:https://doi.org/10.1029/JB093iB06p06463.

Aspinall, W. P. (2006), Structured elicitation of expert judgment for probabilistic hazard and risk assessment in volcanic eruptions, *Statistics in volcanology*, *1*, 15-30.

Aspinall, W. P., A. Bevilacqua, A. Costa, H. Inakura, S. Mahony, A. Neri, & R. S. J. Sparks (2019), Probabilistic reconstruction (or forecasting) of distal runouts of large magnitude ignimbrite PDC flows sensitive to topography using mass-dependent inversion models, paper presented at AGU Fall Meeting 2019, San Francisco, CA, USA.

Barberi, F., M. Coltelli, A. Frullani, M. Rosi, & E. Almeida (1995), Chronology and dispersal characteristics of recently (last 5000 years) erupted tephra of Cotopaxi (Ecuador): implications for long-term eruptive forecasting, *Journal of Volcanology and Geothermal research*, *69*(3-4), 217-239, doi:https://doi.org/10.1016/0377-0273(95)00017-8.

Barberi, F., M. Ghigliotti, G. Macedonio, H. Orellana, M. T. Pareschi, & M. Rosi (1992), Volcanic hazard assessment of Guagua Pichincha (Ecuador) based on past behaviour and numerical models, *J. Volcanol. Geoth. Res.*, *49*(1-2), 53-68, doi:https://doi.org/10.1016/0377-0273(92)90004-W.

Barberi, F., G. Macedonio, M. T. Pareschi, & R. Santacroce (1990), Mapping the tephra fallout risk: an example from Vesuvius, Italy, *Nature*, *344*(6262), 142-144.

Barsotti, S., D. I. Di Rienzo, T. Thordarson, B. B. Björnsson, & S. Karlsdóttir (2018), Assessing impact to infrastructures due to tephra fallout from Öræfajökull volcano (Iceland) by using a scenario-based approach and a numerical model, *Frontiers in Earth Science*, *6*, 196, doi:https://doi.org/10.3389/feart.2018.00196.

Barsotti, S., & A. Neri (2008), The VOL-CALPUFF model for atmospheric ash dispersal: 2. Application to the weak Mount Etna plume of July 2001, *Journal of Geophysical Research: Solid Earth*, *113*(B3), doi:https://doi.org/10.1029/2006JB004624.

Barsotti, S., A. Neri, & J. S. Scire (2008), The VOL-CALPUFF model for atmospheric ash dispersal: 1. Approach and physical formulation, *Journal of Geophysical Research: Solid Earth*, *113*(B3), doi:https://doi.org/10.1029/2006JB004623.

Baxter, P. J. (1990), Medical effects of volcanic eruptions, *Bulletin of Volcanology*, *52*(7), 532-544, doi:https://doi.org/10.1007/BF00301534.

Baxter, P. J., & C. J. Horwell (2015), Impacts of eruptions on human health, in *The encyclopedia of volcanoes*, edited by H. Sigurdsson, B. F. Houghton, S. R. McNutt, H. Rymer and J. Stix, pp. 1035-1047, Elsevier, doi:https://doi.org/10.1016/B978-0-12-385938-9.00060-2.

Bebbington, M. S., S. J. Cronin, I. Chapman, & M. B. Turner (2008), Quantifying volcanic ash fall hazard to electricity infrastructure, *Journal of Volcanology and Geothermal Research*, *177*(4), 1055-1062, doi:https://doi.org/10.1016/j.jvolgeores.2008.07.023.

Bernard, B., J. Battaglia, A. Proaño, S. Hidalgo, F. Vásconez, S. Hernandez, & M. C. Ruiz (2016), Relationship between volcanic ash fallouts and seismic tremor: quantitative assessment of the 2015 eruptive period at Cotopaxi volcano, Ecuador, *Bull. Volc.*, *78*(11), doi:10.1007/s00445-016-1077-5.

Bevilacqua, A., A. Aravena, A. Neri, E. Gutiérrez, D. Escobar, M. Schliz, et al. (2021), Thematic vent opening probability maps and hazard assessment of small-scale pyroclastic density currents in the San Salvador volcanic complex (El Salvador) and Nejapa-Chiltepe volcanic complex (Nicaragua), *Natural Hazards and Earth System Sciences*, *21*(5), 1639-1665, doi:https://doi.org/10.5194/nhess-21-1639-2021.

Bevilacqua, A., A. Bertagnini, M. Pompilio, P. Landi, P. Del Carlo, A. Di Roberto, et al. (2020), Major explosions and paroxysms at Stromboli (Italy): a new historical catalog and temporal models of occurrence with uncertainty quantification, *Scientific Reports*, *10*, doi:https://doi.org/10.1038/s41598-020-74301-8.

Bevilacqua, A., M. I. Bursik, A. K. Patra, B. E. Pitman, Q. Yang, R. Sangani, & S. Kobs-Nawotniak (2018), Late Quaternary eruption record and probability of future volcanic eruptions in the Long Valley volcanic region (CA, USA), *Journal of Geophysical Research: Solid Earth*, *123*(7), 5466-5494, doi:https://doi.org/10.1029/2018JB015644.

Bevilacqua, A., F. Flandoli, A. Neri, R. Isaia, & S. Vitale (2016), Temporal models for the episodic volcanism of Campi Flegrei caldera (Italy) with uncertainty quantification, *Journal of Geophysical Research: Solid Earth*, *121*(11), 7821-7845, doi:https://doi.org/10.1002/2016JB013171.

Bevilacqua, A., R. Isaia, A. Neri, S. Vitale, W. P. Aspinall, M. Bisson, et al. (2015), Quantifying volcanic hazard at Campi Flegrei caldera (Italy) with uncertainty assessment: I. Vent opening maps, *Journal of Geophysical Research: Solid Earth*, *120*, 2309-2329, doi:https://doi.org/10.1002/2014JB011775.

Bevilacqua, A., A. Neri, M. Bisson, T. Esposti Ongaro, F. Flandoli, R. Isaia, et al. (2017), The effects of vent location, event scale, and time forecasts on pyroclastic density current hazard maps at Campi Flegrei caldera (Italy), *Frontiers in Earth Science*, *5*, 72, doi:https://doi.org/10.3389/feart.2017.00072.

Bevilacqua, A., A. K. Patra, M. I. Bursik, E. B. Pitman, J. L. Macías, R. Saucedo, & D. Hyman (2019), Probabilistic forecasting of plausible debris flows from Nevado de Colima (Mexico) using data from the Atenquique debris flow, 1955, *Natural Hazard and Earth System Sciences*, *19*(4), doi:https://doi.org/10.5194/nhess-19-791-2019.

Biass, S., & C. Bonadonna (2011), A quantitative uncertainty assessment of eruptive parameters derived from tephra deposits: the example of two large eruptions of Cotopaxi volcano, Ecuador, *Bulletin of Volcanology*, *73*(1), 73-90.

Biass, S., & C. Bonadonna (2013), A fast GIS-based risk assessment for tephra fallout: the example of Cotopaxi volcano, Ecuador, *Natural Hazards*, *65*(1), 477-495, doi:https://doi.org/10.1007/s11069-012-0378-z.

Biass, S., C. Frischknecht, & C. Bonadonna (2013), A fast GIS-based risk assessment for tephra fallout: the example of Cotopaxi volcano, Ecuador - Part II: vulnerability and risk assessment, *Natural hazards*, *65*(1), 497-521, doi:https://doi.org/10.1007/s11069-012-0457-1.

Biass, S., C. Scaini, C. Bonadonna, A. Folch, K. Smith, & A. Höskuldsson (2014), A multi-scale risk assessment for tephra fallout and airborne concentration from multiple Icelandic volcanoes-Part 1: Hazard assessment, *Natural Hazards and Earth System Sciences*, *14*(8), 2265, doi:10.5194/nhess-14-2265-2014.

Blake, D. M., T. M. Wilson, J. W. Cole, N. I. Deligne, & J. M. Lindsay (2017), Impact of volcanic ash on road and airfield surface skid resistance, *Sustainability*, *9*(8), 1389, doi:https://doi.org/10.3390/su9081389.

Blong, R. J. (1996), Volcanic hazards risk assessment, in *Monitoring and mitigation of volcano hazards*, edited by R. Scarpa and R. I. Tilling, pp. 675-698, Springer, Berlin.

Bonadonna, C. (2006), Probabilistic modelling of tephra dispersion, in *Statistics in Volcanology*, edited by H. M. Mader, S. G. Coles, C. B. Connor and L. J. Connor, pp. 243-259, Geological Society, London.

Bonadonna, C., R. Cioni, M. Pistolesi, M. Elissondo, & V. Baumann (2015a), Sedimentation of long-lasting wind-affected volcanic plumes: the example of the 2011 rhyolitic Cordón Caulle eruption, Chile, *Bulletin of Volcanology*, *77*(2), 13.

Bonadonna, C., C. B. Connor, B. F. Houghton, L. J. Connor, M. Byrne, A. Laing, & T. K. Hincks (2005), Probabilistic modeling of tephra dispersal: Hazard assessment of a multiphase rhyolitic eruption at Tarawera, New Zealand, *Journal of Geophysical Research: Solid Earth*, *110*(B3), doi:https://doi.org/10.1029/2003JB00289.

Bonadonna, C., & J. C. Phillips (2003), Sedimentation from strong volcanic plumes, *Journal of Geophysical Research: Solid Earth*, *108*(B7), doi:https://doi.org/10.1029/2002JB002034.

Bonadonna, C., M. Pistolesi, R. Cioni, W. Degruyter, M. Elissondo, & V. Baumann (2015b), Dynamics of wind-affected volcanic plumes: The example of the 2011 Cordón Caulle eruption, Chile, *Journal of Geophysical Research: Solid Earth*, *120*(4), 2242-2261.

Bonasia, R., L. Capra, A. Costa, G. Macedonio, & R. Saucedo (2011), Tephra fallout hazard assessment for a Plinian eruption scenario at Volcán de Colima (Mexico), *Journal of Volcanology and Geothermal Research*, *203*(1-2), 12-22, doi:https://doi.org/10.1016/j.jvolgeores.2011.03.006.

Brown, S. K., S. F. Jenkins, R. S. J. Sparks, H. Odbert, & M. R. Auker (2017), Volcanic fatalities database: analysis of volcanic threat with distance and victim classification, *Journal of Applied Volcanology*, *6*(1), 1-20, doi:https://doi.org/10.1186/s13617-017-0067-4.

Budd, L., S. Griggs, D. Howarth, & S. Ison (2011), A fiasco of volcanic proportions? Eyjafjallajökull and the closure of European airspace, *Mobilities*, *6*(1), 31-40, doi:https://doi.org/10.1080/17450101.2011.532650.

Bursik, M. I. (2001), Effect of wind on the rise height of volcanic plumes, *Geophysical Research Letters*, *28*(18), 3621-3624, doi:https://doi.org/10.1029/2001GL013393.

Bursik, M. I., M. Jones, S. Carn, K. Dean, A. K. Patra, M. Pavolonis, et al. (2012), Estimation and propagation of volcanic source parameter uncertainty in an ash transport and dispersal model: application to the Eyjafjallajokull plume of 14–16 April 2010, *Bulletin of volcanology*, *74*(10), 2321-2338, doi:https://doi.org/10.1007/s00445-012-0665-2.

Bursik, M. I., S. E. Kobs, A. Burns, O. A. Braitseva, L. I. Bazanova, I. V. Melekestsev, et al. (2009), Volcanic plumes and wind: Jetstream interaction examples and implications for air traffic, *Journal of Volcanology and Geothermal Research*, *186*(1-2), 60-67, doi:https://doi.org/10.1016/j.jvolgeores.2009.01.021.

Capra, L., G. Norini, G. Groppelli, J. L. Macías, & J. L. Arce (2008), Volcanic hazard zonation of the Nevado de Toluca volcano, México, *Journal of Volcanology and Geothermal Research*, *176*(4), 469-484, doi:https://doi.org/10.1016/j.jvolgeores.2008.04.016.

Cioni, R., A. Longo, G. Macedonio, R. Santacroce, A. Sbrana, R. Sulpizio, & D. Andronico (2003), Assessing pyroclastic fall hazard through field data and numerical simulations: example from Vesuvius, *Journal of Geophysical Research: Solid Earth (1978–2012)*, *108*(B2), 2063.

Cooke, R. M. (1991), Experts in uncertainty: opinion and subjective probability in science.

Costa, A., F. Dell'Erba, M. A. Di Vito, R. Isaia, G. Macedonio, G. Orsi, & T. Pfeiffer (2009), Tephra fallout hazard assessment at the Campi Flegrei caldera (Italy), *Bulletin of Volcanology*, *71*(3), 259, doi:https://doi.org/10.1007/s00445-008-0220-3.

Costa, A., G. Macedonio, & A. Folch (2006), A three-dimensional Eulerian model for transport and deposition of volcanic ashes, *Earth and Planetary Science Letters*, *241*(3-4), 634-647, doi:https://doi.org/10.1016/j.epsl.2005.11.019.

Costa, A., L. Pioli, & C. Bonadonna (2016a), Assessing tephra total grain-size distribution: Insights from field data analysis, *Earth and Planetary Science Letters*, *443*, 90-107, doi:https://doi.org/10.1016/j.epsl.2016.02.040.

Costa, A., Y. J. Suzuki, M. Cerminara, B. J. Devenish, T. Esposti Ongaro, M. Herzog, et al. (2016b), Results of the eruptive column model inter-comparison study, *Journal of Volcanology and Geothermal Research*, *326*, 2-25, doi:https://doi.org/10.1016/j.jvolgeores.2016.01.017.

d'Ercole, R., & P. Metzger (2000), La vulnérabilité de Quito (Equateur) face à l'activité du Guagua Pichincha. Les premières leçons d'une crise volcanique durable, *Cahiers Savoisiens de Géographie*, *1*, 39-52, doi:https://hal.archives-ouvertes.fr/hal-01196431.

de' Michieli Vitturi, M., & F. Pardini (2021), PLUME-MoM-TSM 1.0.0: a volcanic column and umbrella cloud spreading model, *Geoscientific Model Development*, *14*(3), 1345–1377, doi:https://doi.org/10.5194/gmd-14-1345-2021.

de'Michieli Vitturi, M., A. Neri, & S. Barsotti (2015), PLUME-MoM 1.0: A new integral model of volcanic plumes based on the method of moments, *Geoscientific Model Development*, *8*(8), 2447.

Ecuatoriana, C. R. (2020), Plan de acción temprana por dispersión de ceniza volcánica. Proyecto Preparación basada en Pronósticos*Rep*.

Eychenne, J., J. L. Le Pennec, L. Troncoso, M. Gouhier, & J. M. Nedelec (2012), Causes and consequences of bimodal grain-size distribution of tephra fall deposited during the August 2006 Tungurahua eruption (Ecuador), *Bulletin of Volcanology*, *74*(1), 187-205, doi:https://doi.org/10.1007/s00445-011-0517-5.

Flandoli, F., E. Giorgi, W. P. Aspinall, & A. Neri (2011), Comparison of a new expert elicitation model with the Classical Model, equal weights and single experts, using a cross-validation technique, *Reliability Engineering & System Safety*, *96*(10), 1292-1310, doi:https://doi.org/10.1016/j.ress.2011.05.012.

Folch, A., A. Costa, & S. Basart (2012), Validation of the FALL3D ash dispersion model using observations of the 2010 Eyjafjallajökull volcanic ash clouds, *Atmospheric Environment*, *48*, 165-183, doi:https://doi.org/10.1016/j.atmosenv.2011.06.072.

Folch, A., A. Costa, & G. Macedonio (2009), FALL3D: A computational model for transport and deposition of volcanic ash, *Computers & Geosciences*, *35*(6), 1334-1342, doi:https://doi.org/10.1016/j.cageo.2008.08.008.

Folch, A., L. Mingari, N. Gutierrez, M. Hanzich, G. Macedonio, & A. Costa (2020), FALL3D-8.0: a computational model for atmospheric transport and deposition of particles, aerosols and radionuclides–Part 1: Model physics and numerics, *Geoscientific Model Development*, *13*(3), 1431-1458, doi:https://doi.org/10.5194/gmd-13-1431-2020.

Folch, A., & R. Sulpizio (2010), Evaluating long-range volcanic ash hazard using supercomputing facilities: application to Somma-Vesuvius (Italy), and consequences for civil aviation over the Central Mediterranean Area, *Bulletin of Volcanology*, *72*(9), 1039-1059, doi:https://doi.org/10.1007/s00445-010-0386-3.

Garcia-Aristizabal, A., H. Kumagai, P. Samaniego, P. Mothes, H. Yepes, & M. Monzier (2007), Seismic, petrologic, and geodetic analyses of the 1999 dome-forming eruption of Guagua Pichincha volcano, Ecuador, *J. Volcanol. Geoth. Res.*, *161*(4), 333-351, doi:https://doi.org/10.1016/j.jvolgeores.2006.12.007.

Gaunt, H. E., B. Bernard, S. Hidalgo, A. Proaño, H. M. Wright, P. Mothes, et al. (2016), Juvenile magma recognition and eruptive dynamics inferred from the analysis of ash time series: The 2015 reawakening of Cotopaxi volcano, *Journal of Volcanology and Geothermal Research*, *328*, 134-146, doi:https://doi.org/10.1016/j.jvolgeores.2016.10.013.

Guffanti, M., G. C. Mayberry, T. J. Casadevall, & R. Wunderman (2009), Volcanic hazards to airports, *Natural hazards*, *51*(2), 287-302, doi:https://doi.org/10.1007/s11069-008-9254-2.

Hall, M. L., P. Mothes, D. Andrade, P. Samaniego, & H. Yepes (2004a), Mapa regional de peligros volcánicos potenciales del volcán Cotopaxi-Zona Sur, IG-EPN, Quito, Ecuador.

Hall, M. L., P. Mothes, P. Samaniego, H. Yepes, & D. Andrade (2004b), Mapa Regional de Peligros Volcánicos Potenciales del Volcán Cotopaxi Zona Norte, IG-EPN, Quito, Ecuador.

Hall, M. L., & P. A. Mothes (2008), The rhyolitic–andesitic eruptive history of Cotopaxi volcano, Ecuador, *Bulletin of Volcanology*, *70*(6), 675-702, doi:https://doi.org/10.1007/s00445-007-0161-2.

Hall, M. L., & C. G. M. von Hillebrandt (1988a), Mapa de los peligros volcanicos potenciales asociados con el volcan Cotopaxi: zona norte and zona sur, IG-EPN, Quito, Ecuador.

Hall, M. L., & C. G. M. von Hillebrandt (1988b), Mapa de los peligros volcanicos potenciales asociados con el volcan Guagua Pichincha-Provincia de Pichincha, IG-EPN, Quito, Ecuador.

Hersbach, H., B. Bell, P. Berrisford, S. Hirahara, A. Horányi, J. Muñoz-Sabater, et al. (2020), The ERA5 global reanalysis, *Q. J. Roy. Meteor. Soc.*, *146*(730), 1999-2049.

Hidalgo, S., J. Battaglia, S. Arellano, D. Sierra, B. Bernard, R. Parra, et al. (2018), Evolution of the 2015 Cotopaxi eruption revealed by combined geochemical and seismic observations, *Geochemistry, Geophysics, Geosystems*, *19*(7), 2087-2108, doi:https://doi.org/10.1029/2018GC007514.

Hurst, T., & W. Smith (2004), A Monte Carlo methodology for modelling ashfall hazards, *Journal of volcanology and geothermal research*, *138*(3-4), 393-403, doi:https://doi.org/10.1016/j.jvolgeores.2004.08.001.

IG-EPN, IGM, & IRD (2019), Mapa de Peligros Volcánicos Potenciales del Volcán Guagua Pichincha 3ra. Edición, Quito - Ecuador, Quito - Ecuador.

Kalnay, E., M. Kanamitsu, R. Kistler, W. Collins, D. Deaven, L. Gandin, et al. (1996), The NCEP/NCAR 40-Year Reanalysis Project, *Bull. Am. Met. Soc.*, *77*(3), 437-472, doi:10.1175/1520-0477(1996)077<0437:tnyrp>2.0.co;2.

López, A., J. Ramírez, F. Vásconez, B. Bernard, F. Valencia, S. Hidalgo, et al. (2016), Volcanic ash impacts on the dielectric strength of HVAC Outdoor Suspension Insulators: the case of Cotopaxi and Tungurahua volcanoes (Ecuador), paper presented at Cities on Volcanoes 9, Puerto Varas, Chile, 20-25/11/2016.

Macedonio, G., & A. Costa (2012), Brief Communication" Rain effect on the load of tephra deposits", *Natural Hazards and Earth System Sciences*, *12*(4), 1229-1233, doi:https://doi.org/10.5194/nhess-12-1229-2012.

Macedonio, G., A. Costa, & A. Longo (2005), A computer model for volcanic ash fallout and assessment of subsequent hazard, *Computers & Geosciences*, *31*(7), 837-845, doi:https://doi.org/10.1016/j.cageo.2005.01.013.

Macedonio, G., A. Costa, S. Scollo, & A. Neri (2016), Effects of eruption source parameter variation and meteorological dataset on tephra fallout hazard assessment: example from Vesuvius (Italy), *Journal of Applied Volcanology*, *5*(1), 1.

Macedonio, G., M. T. Pareschi, & R. Santacroce (1988), A numerical simulation of the Plinian fall phase of 79 AD eruption of Vesuvius, *Journal of Geophysical Research: Solid Earth*, *93*(B12), 14817-14827.

Madankan, R., S. Pouget, P. Singla, M. I. Bursik, J. Dehn, M. Jones, et al. (2014), Computation of probabilistic hazard maps and source parameter estimation for volcanic ash transport and dispersion, *Journal of Computational Physics*, *271*, 39-59, doi:https://doi.org/10.1016/j.jcp.2013.11.032.

Martel, C., J. Andújar, P. Mothes, B. Scaillet, M. Pichavant, & I. Molina (2018), Storage conditions of the mafic and silicic magmas at Cotopaxi, Ecuador, *Journal of Volcanology and Geothermal Research*, *354*, 74-86.

Marzocchi, W., L. Sandri, & J. Selva (2008), BET_EF: a probabilistic tool for long-and short-term eruption forecasting, *Bulletin of Volcanology*, *70*(5), 623-632, doi:https://doi.org/10.1007/s00445-007-0157-y.

Marzocchi, W., L. Sandri, & J. Selva (2010), BET_VH: a probabilistic tool for long-term volcanic hazard assessment, *Bulletin of Volcanology*, *72*(6), 705-716, doi:https://doi.org/10.1007/s00445-010-0357-8.

Mastin, L. G., M. Guffanti, R. Servranckx, P. Webley, S. Barsotti, K. Dean, et al. (2009), A multidisciplinary effort to assign realistic source parameters to models of volcanic ash-cloud transport and dispersion during eruptions, *Journal of Volcanology and Geothermal Research*, *186*(1-2), 10-21, doi:https://doi.org/10.1016/j.jvolgeores.2009.01.008.

Mastin, L. G., A. R. Van Eaton, D. Schneider, & R. P. Denlinger (2017), Ongoing Efforts to Make Ash-Cloud Model Forecasts More Accurate*Rep.*, NATO Science and Technology Organization.

Miller, C. D., D. R. Mullineaux, & M. L. Hall (1978), Reconnaissance Map of Potential Volcanic Hazards from Cotopaxi Volcano, Ecuador: Mapa de Reconocimiento de Riesgos Volganicos Potenciales Del Volcan Cotopaxi, Ecuador, US Geological Survey.

Mothes, P. A., P. Espin, M. L. Hall, F. Vasconez, D. Sierra, & D. Andrade (2016a), Mapa regional de amenazas volcánicas potenciales del volcán Cotopaxi, zona Norte, Quito.

Mothes, P. A., P. Espin, M. L. Hall, F. Vasconez, D. Sierra, & D. Andrade (2016b), Mapa regional de amenazas volcánicas potenciales del volcán Cotopaxi, zona Sur, Quito.

Neri, A., W. P. Aspinall, R. Cioni, A. Bertagnini, P. J. Baxter, G. Zuccaro, et al. (2008), Developing an event tree for probabilistic hazard and risk assessment at Vesuvius, *Journal of Volcanology and Geothermal Research*, *178*(3), 397-415, doi:https://doi.org/10.1016/j.jvolgeores.2008.05.014.

1141 Neri, A., A. Bevilacqua, T. Esposti Ongaro, R. Isaia, W. P. Aspinall, M. Bisson, et al. (2015), Quantifying volcanic
1142 hazard at Campi Flegrei caldera (Italy) with uncertainty assessment: II. Pyroclastic density current invasion
1143 maps, *Journal of Geophysical Research: Solid Earth*, doi:https://doi.org/10.1002/2014JB011776.
1144 NOAA (2004), Global Data Assimilation System (GDAS1) Archive Information, edited,
1145 doi:https://www.ready.noaa.gov/gdas1.php.
1146 Orsi, G., M. A. Di Vito, & R. Isaia (2004), Volcanic hazard assessment at the restless Campi Flegrei caldera,
1147 *Bulletin of Volcanology*, *66*(6), 514-530, doi:https://doi.org/10.1007/s00445-003-0336-4.
1148 Pardini, F., S. Corradini, A. Costa, T. Esposti Ongaro, L. Merucci, A. Neri, & D. Stelitano (2020), Ensemble-Based
1149 Data Assimilation of Volcanic Ash Clouds from Satellite Observations: Application to the 24 December
1150 2018 Mt. Etna Explosive Eruption, *Atmosphere*, *11*(4), 359, doi:https://doi.org/10.3390/atmos11040359.
1151 Patra, A. K., A. Bevilacqua, A. Akhavan-Safaei, E. B. Pitman, M. I. Bursik, & D. Hyman (2020), Comparative
1152 analysis of the structures and outcomes of geophysical flow models and modeling assumptions using
1153 uncertainty quantification, *Frontiers in Earth Science*, doi:10.3389/feart.2020.00275.
1154 Patra, A. K., A. Bevilacqua, & A. A. Safei (2018), Analyzing Complex Models using Data and Statistics, paper
1155 presented at International Conference on Computational Science, Springer.
1156 Pistolesi, M., M. Rosi, R. Cioni, K. V. Cashman, A. Rossotti, & E. Aguilera (2011), Physical volcanology of the
1157 post–twelfth-century activity at Cotopaxi volcano, Ecuador: Behavior of an andesitic central volcano, *Geol.*
1158 *Soc. Am. Bull.*, *123*(5-6), 1193-1215, doi:https://doi.org/10.1130/B30301.1.
1159 Pouget, S., M. I. Bursik, P. Singla, & T. Singh (2016), Sensitivity analysis of a one-dimensional model of a volcanic
1160 plume with particle fallout and collapse behavior, *Journal of Volcanology and Geothermal Research*, *326*,
1161 43-53, doi:https://doi.org/10.1016/j.jvolgeores.2016.02.018.
1162 Prata, A. T., L. Mingari, A. Folch, G. Macedonio, & A. Costa (2021), FALL3D-8.0: a computational model for
1163 atmospheric transport and deposition of particles, aerosols and radionuclides–Part 2: model validation,
1164 *Geoscientific Model Development*, *14*(1), 409-436, doi:https://doi.org/10.5194/gmd-14-409-2021.
1165 Riley, C. M., W. I. Rose, & G. J. S. Bluth (2003), Quantitative shape measurements of distal volcanic ash, *Journal*
1166 *of Geophysical Research: Solid Earth*, *108*(B10), doi:https://doi.org/10.1029/2001JB000818.
1167 Robin, C., P. Samaniego, J. L. Le Pennec, M. Fornari, P. Mothes, & J. Van Der Plicht (2010), New radiometric and
1168 petrological constraints on the evolution of the Pichincha volcanic complex (Ecuador), *Bulletin of*
1169 *volcanology*, *72*(9), 1109-1129, doi:https://doi.org/10.1007/s00445-010-0389-0.
1170 Robin, C., P. Samaniego, J. L. Le Pennec, P. Mothes, & J. van der Plicht (2008), Late Holocene phases of dome
1171 growth and Plinian activity at Guagua Pichincha volcano (Ecuador), *Journal of Volcanology and*
1172 *Geothermal Research*, *176*(1), 7-15, doi:https://doi.org/10.1016/j.jvolgeores.2007.10.008.
1173 Rose, A. N., J. J. McKee, K. M. Sims, E. A. Bright, A. E. Reith, & M. L. Urban (2020), LandScan 2019, edited, Oak
1174 Ridge National Laboratory, Oak Ridge, TN, doi:https://landscan.ornl.gov/.
1175 Rutarindwa, R., E. T. Spiller, A. Bevilacqua, M. I. Bursik, & A. K. Patra (2019), Dynamic probabilistic hazard
1176 mapping in the Long Valley Volcanic Region CA: integrating vent opening maps and statistical surrogates
1177 of physical models of pyroclastic density currents, *J. Geophys. Res.-Sol. Ea.*
1178 Samaniego, P., C. Robin, G. Chazot, E. Bourdon, & J. Cotten (2010), Evolving metasomatic agent in the Northern
1179 Andean subduction zone, deduced from magma composition of the long-lived Pichincha volcanic complex
1180 (Ecuador), *Contributions to Mineralogy and Petrology*, *160*(2), 239-260,
1181 doi:https://doi.org/10.1007/s00410-009-0475-5.
1182 Sandri, L., A. Costa, J. Selva, R. Tonini, G. Macedonio, A. Folch, & R. Sulpizio (2016), Beyond eruptive scenarios:
1183 assessing tephra fallout hazard from Neapolitan volcanoes, *Scientific reports*, *6*(1), 1-13,
1184 doi:https://doi.org/10.1038/srep24271.
1185 Scaini, C., A. Folch, & M. Navarro (2012), Tephra hazard assessment at Concepción Volcano, Nicaragua, *Journal*
1186 *of volcanology and geothermal research*, *219*, 41-51, doi:https://doi.org/10.1016/j.jvolgeores.2012.01.007.
1187 Schwaiger, H. F., R. P. Denlinger, & L. G. Mastin (2012), Ash3d: A finite-volume, conservative numerical model
1188 for ash transport and tephra deposition, *Journal of Geophysical Research: Solid Earth*, *117*(B4),
1189 doi:https://doi.org/10.1029/2011JB008968.
1190 Scollo, S., S. Tarantola, C. Bonadonna, M. Coltelli, & A. Saltelli (2008), Sensitivity analysis and uncertainty
1191 estimation for tephra dispersal models, *Journal of Geophysical Research: Solid Earth*, *113*(B6),
1192 doi:https://doi.org/10.1029/2006JB004864.
1193 Sparks, R. S. J., M. I. Bursik, S. N. Carey, J. S. Gilbert, L. S. Glaze, H. Sigurdsson, & A. W. Woods (1997),
1194 *Volcanic plumes*, Wiley.

Spence, R. J. S., I. Kelman, P. J. Baxter, G. Zuccaro, & S. Petrazzuoli (2005), Residential building and occupant vulnerability to tephra fall, *Natural Hazards and Earth System Sciences*, *5*(4), 477-494, doi:https://doi.org/10.5194/nhess-5-477-2005.

Spera, F. J. (2000), Physical properties of magma, in *Encyclopedia on Volcanoes*, edited by H. Sigurdsson, B. F. Houghton, S. R. McNutt, H. Rymer and J. Stix, Academic Press, San Diego, CA.

Stefanescu, E. R., A. K. Patra, M. I. Bursik, R. Madankan, S. Pouget, M. Jones, et al. (2014), Temporal, probabilistic mapping of ash clouds using wind field stochastic variability and uncertain eruption source parameters: Example of the 14 A pril 2010 E yjafjallajökull eruption, *Journal of Advances in Modeling Earth Systems*, *6*(4), 1173-1184, doi:https://doi.org/10.1002/2014MS000332.

Stein, A. F., R. R. Draxler, G. D. Rolph, B. J. B. Stunder, M. D. Cohen, & F. Ngan (2015), NOAA's HYSPLIT atmospheric transport and dispersion modeling system, *Bulletin of the American Meteorological Society*, *96*(12), 2059-2077.

Tadini, A., A. Bevilacqua, A. Neri, R. Cioni, W. P. Aspinall, M. Bisson, et al. (2017a), Assessing future vent opening locations at the Somma-Vesuvio volcanic complex: 2. Probability maps of the caldera for a future Plinian/sub-Plinian event with uncertainty quantification, *Journal of Geophysical Research: Solid Earth*, *122*(6), 4357-4376, doi:10.1002/2016JB013860.

Tadini, A., M. Bisson, A. Neri, R. Cioni, A. Bevilacqua, & W. P. Aspinall (2017b), Assessing future vent opening locations at the Somma-Vesuvio volcanic complex: 1. A new information geo-database with uncertainty characterizations, *Journal of Geophysical Research: Solid Earth*, *122*(6), 4336-4356, doi:10.1002/2016JB013858.

Tadini, A., O. Roche, P. Samaniego, N. Azzaoui, A. Bevilacqua, A. Guillin, et al. (2021), Eruption type probability and eruption source parameters at Cotopaxi and Guagua Pichincha volcanoes (Ecuador) with uncertainty quantification, *Bullettin of Volcanology*, *83*(35), doi:https://doi.org/10.1007/s00445-021-01458-z.

Tadini, A., O. Roche, P. Samaniego, A. Guillin, N. Azzaoui, M. Gouhier, et al. (2020), Quantifying the uncertainty of a coupled plume and tephra dispersal model: PLUME-MOM/HYSPLIT simulations applied to Andean volcanoes, *Journal of Geophysical Research: Solid Earth*, *125*(2), doi:https://doi.org/10.1029/2019JB018390.

Tsuji, T., M. Ikeda, H. Kishimoto, K. Fujita, N. Nishizaka, & K. Onishi (2017), Tephra Fallout Hazard Assessment for VEI5 Plinian Eruption at Kuju Volcano, Japan, Using TEPHRA2, paper presented at IOP Conference Series: Earth and Environmental Science, IOP Publishing.

Tsunematsu, K., & C. Bonadonna (2015), Grain-size features of two large eruptions from Cotopaxi volcano (Ecuador) and implications for the calculation of the total grain-size distribution, *Bulletin of Volcanology*, *77*(7), 64, doi:https://doi.org/10.1007/s00445-015-0949-4.

Vasconez, F., D. Sierra, M. Almeida, D. Andrade, J. M. Marrero, P. A. Mothes, et al. (2017), Mapa preliminar de amenazas potenciales del volcán Cotopaxi—Zona oriental, IG-EPN, Quito, Ecuador.

Vázquez, R., R. Bonasia, A. Folch, J. L. Arce, & J. L. Macías (2019), Tephra fallout hazard assessment at Tacaná volcano (Mexico), *Journal of South American Earth Sciences*, *91*, 253-259, doi:https://doi.org/10.1016/j.jsames.2019.02.013.

Volentik, A. C. M., & B. F. Houghton (2015), Tephra fallout hazards at Quito International Airport (Ecuador), *Bulletin of Volcanology*, *77*(6), 50, doi:https://doi.org/10.1007/s00445-015-0923-1.

Wilson, G., T. M. Wilson, N. I. Deligne, & J. W. Cole (2014), Volcanic hazard impacts to critical infrastructure: A review, *Journal of Volcanology and Geothermal Research*, *286*, 148-182, doi:https://doi.org/10.1016/j.jvolgeores.2014.08.030.

Wilson, T. M., C. Stewart, V. Sword-Daniels, G. S. Leonard, D. M. Johnston, J. W. Cole, et al. (2012), Volcanic ash impacts on critical infrastructure, *Physics and Chemistry of the Earth, Parts A/B/C*, *45*, 5-23, doi:https://doi.org/10.1016/j.pce.2011.06.006.

Wolf, T. (1904), *Crónica de los fenómenos volcánicos y terremotos en el Ecuador con algunas noticias sobre otros países de la América Central y Meridional desde 1535 hasta 1797*, Imprenta de la Universidad Central de Quito, Quito, doi:http://www.dspace.uce.edu.ec/handle/25000/14200.

Wright, H. M. N., K. V. Cashman, M. Rosi, & R. Cioni (2007), Breadcrust bombs as indicators of Vulcanian eruption dynamics at Guagua Pichincha volcano, Ecuador, *Bulletin of Volcanology*, *69*(3), 281-300, doi:https://doi.org/10.1007/s00445-006-0073-6.

Yang, Q., E. B. Pitman, M. I. Bursik, & S. F. Jenkins (2021), Tephra deposit inversion by coupling Tephra2 with the Metropolis-Hastings algorithm: algorithm introduction and demonstration with synthetic datasets, *Journal of Applied Volcanology*, *10*(1), 1-24, doi:https://doi.org/10.1186/s13617-020-00101-4.

Yang, Q., E. B. Pitman, E. T. Spiller, M. I. Bursik, & A. Bevilacqua (2020), Novel statistical emulator construction for volcanic ash transport model Ash3d with physically motivated measures, *Proceedings of the Royal Society A*, *476*(2242), 20200161, doi:https://doi.org/10.1098/rspa.2020.0161.

## References from the supporting information

Tadini, A., O. Roche, P. Samaniego, N. Azzaoui, A. Bevilacqua, A. Guillin, et al. (2021), Eruption type probability and eruption source parameters at Cotopaxi and Guagua Pichincha volcanoes (Ecuador) with uncertainty quantification, *Bullettin of Volcanology*, *83*(35), doi:https://doi.org/10.1007/s00445-021-01458-z.